

SILTSTONES ACROSS THE *DAPTOCEPHALUS* (*DICYNODON*) AND *LYSTROSAURUS* ASSEMBLAGE ZONES, KAROO BASIN, SOUTH AFRICA, SHOW NO EVIDENCE FOR ARIDIFICATION

JIAWEN LI,¹ ROBERT A. GASTALDO,¹ JOHANN NEVELING,² AND JOHN W. GEISSMAN³

¹ Department of Geology, Colby College, Waterville, Maine 04901, U.S.A.

² Council for Geosciences, Private Bag x112, Silverton, Pretoria 0001, South Africa

³ Department of Geosciences, The University of Texas at Dallas, Richardson, Texas 75080, U.S.A.

e-mail: ragastal@colby.edu

ABSTRACT: Changes in the record of vertebrate-assemblage zones in the Karoo Basin, South Africa, serve as a model for the response of terrestrial ecosystems to the end-Permian biotic crisis. Vertebrate turnover from the *Daptocephalus* to *Lystrosaurus* Assemblage Zone is believed to have begun with the appearance of subtle siltstone-color variance and is coeval with a unique, laminated lithofacies, both of which are interpreted by other workers to represent evidence for an aridification trend. The laminated facies consists of interbedded greenish-gray and dark reddish-gray siltstone, with coloration of the latter reported as a function of an increasing eolian component. The current study combines stratigraphy, petrography, geochemistry, and rock magnetic properties of an interlaminated succession and lateral equivalents at Old Lootsberg Pass in the Eastern Cape Province to determine whether such subtle color variance is a function of aridification and, hence, climate change.

Siltstones were evaluated from intervals both below and above a pedogenic nodule-bearing feldspathic wacke that is physically correlated over a > 0.5 km distance. The lower succession consists of interbedded greenish-gray (*sensu latu*) and reddish-gray (*sensu latu*) siltstone in which undisturbed and minimally disturbed primary sedimentary, along with few secondary biogenic structures, are interpreted to represent deposition in an abandoned channel-fill complex. Massive greenish-gray and dark reddish-gray siltstone above the channel complex demonstrate that coloration is variable across laterally equivalent strata. Both lithologies were assessed using X-ray fluorescence, X-ray diffraction, Mössbauer spectroscopy, scanning electron microscopy with EDS, and bulk magnetic susceptibility, stepwise acquisition of an isothermal remanent magnetization (IRM), and backfield direct field demagnetization.

Our data indicate that there is no statistically significant difference in major-element concentrations between lithologies and that subtle color difference is a function of the presence of fine (< 1 wt. %) hematite in the reddish-gray rocks. Hence, the abundance of Fe is not responsible for either color. Rather, hematite is found to be localized as reticulate, surficial coatings on both illite and chlorite flakes, the only two clay species identified in the study. Similarly, there is no clear distinction in the magnetic mineralogy of sample suites; both magnetite and maghemite vary in abundance. These data lead to an interpretation that the presence of hematite is early diagenetic and the landscape in the earliest part of the *Lystrosaurus* Assemblage Zone was not arid. In contrast, the landscape was wet, that allowed for the continued growth of a Permian-age flora under conditions of high water table that experienced temporal fluxes in the hydrological regime promoting spatial color modification of sediment.

INTRODUCTION

The Permian–Triassic Mass Extinction (PTME) is considered the most catastrophic biodiversity loss of the Phanerozoic. The crisis currently is dated to between 251.941 ± 0.037 and 251.880 ± 0.031 Ma in the marine realm (Burgess et al. 2014) where the stratigraphic record includes invertebrate fossil assemblages associated with stable-isotope trends. Combined, the marine records enable a comprehensive understanding of the environmental changes documented across the crisis and, thus, infer possible causes and processes affecting the PTME in the latest Paleozoic oceans (Payne and Clapham 2012). In contrast, the latest Permian terrestrial rock record provides a far less robust and detailed resolution of time (Gastaldo et al. 2015). This is because terrestrial successions are both incomplete, due to long periods of landscape stasis and erosion, and

modified by climatic and environmental conditions after deposition (DiMichele and Gastaldo 2008; Gastaldo and Demko 2011). In addition, terrestrial successions spanning the PTME are geographically limited to exposures in Spain, Germany, Russia, Antarctica, East India, Australia, South China, west Texas (USA), and South Africa (Doornenbal and Stevenson 2010; Benton and Newell 2014). Of these localities, the Karoo Basin, South Africa, is considered the most accessible. Here, the most complete latest Permian–earliest Triassic stratigraphic record is reported to be exposed and has been identified principally as a function of vertebrate biostratigraphy (Smith and Botha-Brink 2014; Rubidge et al. 2016; Viglietti et al. 2016; Fig. 1A).

Changes in vertebrate assemblage zones in the Karoo Basin, in conjunction with chemostratigraphy (MacLeod et al. 2000; Rey et al.

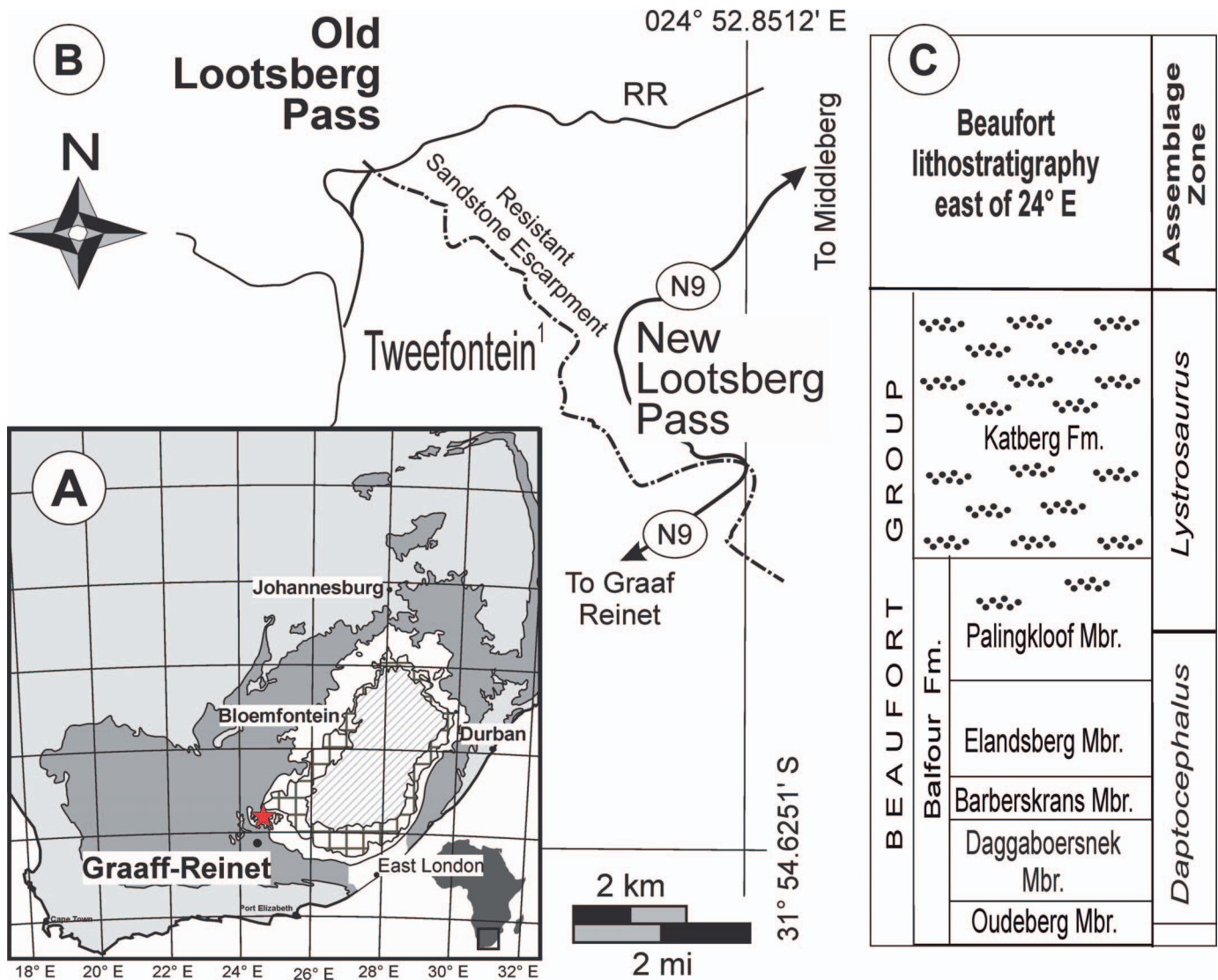


FIG. 1.—Locality maps. **A**) Generalized map of southern Africa on which Old Lootsberg Pass is located with a star north of the town of Graaff-Reinet. The outline of the Karoo Basin is in dark gray, exposures of the *Daptocephalus* (formerly *Dicynodon*; Viglietti et al. 2016) Assemblage Zone are in white, distribution of the *Lystrosaurus* Assemblage Zone is cross hatched, and overlying vertebrate biozones in diagonal lines. Bloemfontein, Durban, East London, and Johannesburg provide geographical reference points. **B**) Map showing the geographic relationship between three localities—Old (West) Lootsberg Pass, Tweefontein, and (East) Lootsberg Pass—on which the current terrestrial PTME model is based (Ward et al. 2000; Ward et al. 2005; Smith and Botha-Brink 2014). Locality used in the current study is in **bold**. RR, railroad. **C**) Generalized stratigraphy of lithologic units and vertebrate assemblage zones in the area.

2016) and magnetostratigraphy (De Kock and Kirschvink 2004; Ward et al. 2005), have been widely accepted as representing the terrestrial response to the PTME (Smith and Botha-Brink 2014; Rubidge et al. 2016; Viglietti et al. 2016). These interpretations, in part, have been a consequence of a reported absence of datable volcanism-related deposits near the vertebrate-defined boundary (Ward et al. 2005; Erwin 2006). This boundary has been associated with the replacement of the *Daptocephalus* Assemblage Zone (AZ; recently renamed by Viglietti et al. 2016) by the *Lystrosaurus* AZ, and interpreted to have been coeval with the marine extinction event (Ward et al. 2005; Smith and Botha-Brink 2014). Recently, Gastaldo et al. (2015) reported the first high-precision U-Pb ID-TIMS age from a porcellanite in strata constituting a boundary-zone sequence from the Karoo Supergroup, and this age determination suggests that this vertebrate turnover occurred in the early Changhsingian rather than the latest Changhsingian. This age assignment for the biozone turnover is significantly older than the marine extinction event, and Gastaldo et al. (2015) reasoned that the expression of

the terrestrial Permian–Triassic Boundary (PTB) should be stratigraphically higher and, thus, not correlated with the vertebrate turnover as currently recognized. Nonetheless, the vertebrate-defined PTB remains widely recognized and continues to be used in published literature (Rey et al. 2016; Rubidge et al. 2016; Viglietti et al. 2016).

The rock succession straddling the reported biozone turnover and interpreted terrestrial PTB is dominated by siltstone with subordinate sandstone, both representing deposition in a fully terrestrial setting (Johnson et al. 2006). Siltstone beds are interpreted as overbank paleosols (Retallack et al. 2003; Gastaldo and Rolerson 2008; Smith and Botha-Brink 2014), whereas sandstone bodies are fluvial deposits. Both a change in subtle siltstone color, from olive-gray to maroon (Ward et al. 2000; Ward et al. 2005), and fluvial architecture (Smith and Ward 2001), from meandering to anabranching systems, have been interpreted to be associated with rapid climate change. The current PTME model envisions this change as a general drying, reflected in siltstone rubification (Smith

and Ward 2001; Ward et al. 2005), to arid conditions immediately before the turnover in vertebrate assemblages (Smith and Botha-Brink 2014). The same shift in siltstone coloration is reported from elsewhere (e.g., Russia), and extrapolation of this phenomenon has been used to infer a global climatic shift (Benton and Newell 2014).

Siltstone coloration is held to be a function of the $\text{Fe}^{2+}/\text{Fe}^{3+}$ ratio in the sediment before compaction and lithification, and is believed in the Karoo Basin to reflect the oxidizing potential of the depositional environment (Coney et al. 2007; Smith and Botha-Brink 2014). Greenish coloration, a result from the dominance of Fe^{2+} , is associated with a moist climate and high water table that insulates iron in subaerial sediments from oxidation by atmospheric oxygen. A more reddish coloration, on the other hand, is interpreted to represent a high proportion of Fe^{3+} oxidized by direct contact with air in a dry climate with a low water table (Turner 1980; Coney et al. 2007). Although other researchers have reported that sediment reddening is not necessarily correlated with climate (e.g., Sheldon 2005), this interpretation continues to be applied to the Karoo succession. The question remains whether the reported subtle change in siltstone color across the *Daptocephalus* to *Lystrosaurus* Assemblage Zones is actually due to appreciable differences in the $\text{Fe}^{2+}/\text{Fe}^{3+}$ ratio or some other characteristic of these rocks. And, if so, are such ratios the result of the climatic and environmental conditions during and/or soon after silt deposition? If not, what geochemical and/or mineralogical properties of the rocks are responsible for the subtle shift in color, and to what conditions prevailing at the time of deposition are these properties linked?

A suite of greenish-gray and reddish-gray siltstones, collected in a stratigraphic framework from the succession of rocks spanning the *Daptocephalus* to *Lystrosaurus* turnover at Old Lootsberg Pass, are analyzed to determine whether the change in color is a reflection of aridification. Analytical techniques employed include petrographic thin-section examination, X-ray fluorescence and X-ray diffraction, Mössbauer spectroscopy, SEM with EDS, and analysis of rock magnetic properties. Data indicate that primary sedimentary structures in both siltstone suites are indicative of a fluvial origin, and that most major elements in the various colored sample suites are statistically indistinguishable. The presence of finely dispersed hematite, which we interpret to be of early diagenetic origin, is responsible, rather than a lower bulk $\text{Fe}^{2+}/\text{Fe}^{3+}$ ratio, for color alteration to dark reddish-gray in this succession.

GENERAL GEOLOGIC SETTING

The Karoo Supergroup was deposited in a basin fronting the emerging Cape Fold belt, with sedimentation starting in the Pennsylvanian and continuing into the Jurassic (Johnson et al. 2006). Fully continental deposits characterize the Middle Permian–Lower (Rubidge et al. 2000) or Upper (Ottone et al. 2014) Triassic Beaufort Group, subdivided into the basal Adelaide and overlying Tarkastad subgroups. At the contact between these two subgroups, meandering fluvial and lacustrine deposits incised into widespread Permian paleosols (Smith 1995) were replaced by braidplain systems (Ward et al. 2000; Ward et al. 2005; Smith and Botha-Brink 2014) and paleosols (Smith 1995; Retallack et al. 2003) assigned to the early Triassic. Grayish paleosols in siltstone intervals, widely considered to represent pre-extinction soils (Smith and Botha-Brink 2014), are differentiated from so-called post-extinction paleosols described as predominantly maroon in color. The stratigraphically lowest occurrence of siltstone reddening over this interval is reported to be in the Palingkloof Member, the uppermost member of the Balfour Formation (Adelaide Subgroup), wherein the vertebrate-defined PTB has been repeatedly reported to exist (Ward et al. 2000; Ward et al. 2005; Smith and Botha-Brink 2014; Rubidge et al. 2016). Strata representing the traditionally defined vertebrate-extinction event in the lower half of the Palingkloof Member are overlain by fluvial complexes assigned to the Lower Triassic Katberg Formation. The Katberg Formation is defined as an arenaceous-

dominated sequence (Johnson et al. 2006) in which intraformational clast- and matrix-supported pedogenic nodule-conglomerate lag deposits occur with mud-chip conglomerate characterized by mudclast aggregates (Gastaldo et al. 2013). Neveling et al. (2016) recently have questioned the practicality of using the conglomerate lithofacies as a diagnostic criterion for the formation (Neveling et al. 2016).

LOCALITY

Old Lootsberg Pass, in the Eastern Cape Province, South Africa, is northeast of Graaf-Reinet, and located on the Blaauwater 65 farm (S31° 47.771', E024° 47.861'; Fig. 1). It is one of eleven stratigraphic sequences in which the vertebrate-defined PTB is reported to occur in the Karoo Basin (Ward et al. 2000; Ward et al. 2005; Smith and Botha-Brink 2014). Exposures in the area are easy to locate, and are exposed either in erosional gullies (dongas) or as outcrop that parallels the dirt roadway and railroad, once used to traverse the mountain escarpment. Here, Gastaldo et al. (2015) documented an ~ 150 m stratigraphic section through the upper *Daptocephalus* and lower *Lystrosaurus* Assemblage Zones and measured 11 sections across the interval marking the biozone transition (Gastaldo et al. 2017). These 11 sections are correlated using the upper bounding surfaces of thick sandstone bodies containing intraformational, pedogenic nodule conglomerate, previously considered to be a diagnostic lithofacies of the Katberg Formation (Botha and Smith 2006; Smith and Botha-Brink 2014). These sandstones can be traced laterally for at least one kilometer (Figs. 2, 3), as demonstrated by Gastaldo et al. (2015).

The stratigraphic position of the boundary between the *Daptocephalus* and *Lystrosaurus* Assemblage Zones lies somewhere in this interval. Using Smith and Botha-Brink's (2014) database with vertebrate-GPS coordinates (R. Smith, personal communication, 2014), the biozone boundary lies ~ 15 m below the base of the intraformational-conglomerate-bearing sandstone that Gastaldo et al. (2015; Fig. 3) have used as one correlation datum. The occurrence of a characteristic dicynodontoid skull, most likely belonging to a taxon from the *Daptocephalus* Assemblage Zone (Gastaldo et al. 2017), in a basal pedogenic conglomerate-lag deposit above that stratigraphic position led Gastaldo et al. (2015) to raise the biozone boundary to at least the base of that specific sandstone body. *Lystrosaurid* fossils, including *L. murrayi* and *L. declivis* assigned to the *Lystrosaurus* Assemblage Zone (Botha and Smith 2007), are preserved in the interval overlying these channel bedform deposits (Gastaldo et al. 2017), supporting their contention. Yet, both of the biozone-boundary positions are in stark contrast to Ward et al.'s (2005) reported placement, which appears to lie higher in the *Lystrosaurus* Assemblage Zone (Figs. 2, 3).

MATERIALS AND METHODS

Stratigraphic sections were measured using standard field techniques and a Jacob's staff with Abney level. We have characterized 11 measured sections, the sum total of which is ~ 700 m, and correlated them by walking bounding surfaces of laterally extensive sandstone bodies across the area (Fig. 2). GPS coordinates were taken every 50 to 100 paces on each bounding surface and plotted using Google Earth to confirm the geographic relationships among sandstone units. Lithologic field descriptions follow our previously published studies (e.g., Prevec et al. 2010; Gastaldo et al. 2014). Here, we note that discrepancies in nomenclature of the same Munsell color designations exist between the Geological Society of America's Rock-Color Chart (2008) and the Munsell Soil-Color Chart (2000). We have used the Rock-Color Chart when referencing color in this, and previous, reports. Hand samples from intervals of thin, interbedded greenish- and reddish-gray siltstone successions, and from massive, single-colored siltstone beds were collected; most samples (N = 23) originate from section 10 and span a stratigraphic distance of 30 m. In contrast, four

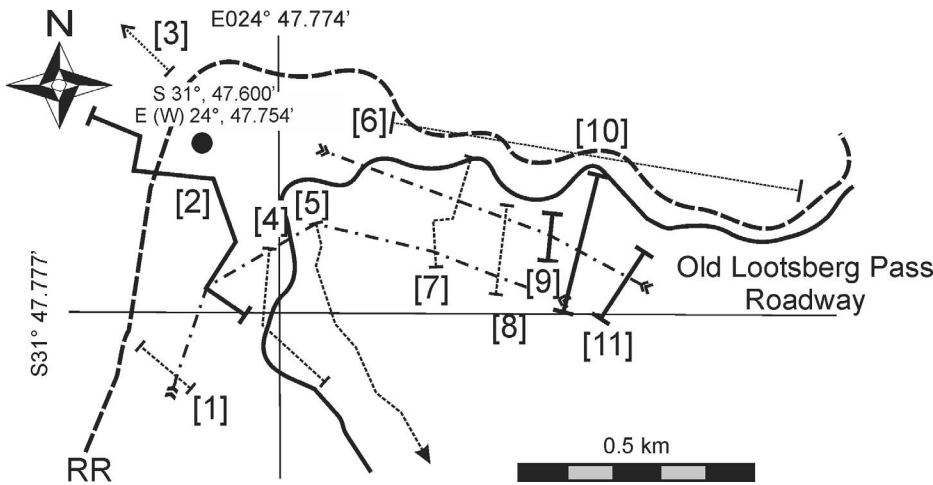


Fig. 2.—Eleven measured stratigraphic sections used to characterize vertical and lateral facies relationships at Old Lootsberg Pass. Stratigraphic sections over which greenish-gray and reddish-gray siltstone were sampled (sections 2, 9, 10, 11) are indicated by bold, end-capped lines. Dotted-and-dashed lines with feathered ends illustrate thick, fine-grained wacke bodies, the bounding surfaces of which are traced physically and used as correlative datums. GPS coordinates (WGS 84 standard) for the Old Lootsberg Pass section, as reported by Ward et al. (2000), corrected for longitude, appear as a solid black dot; GPS coordinates for the base of the four sampled sections are provided in Figure 3. Scale is 0.5 km.

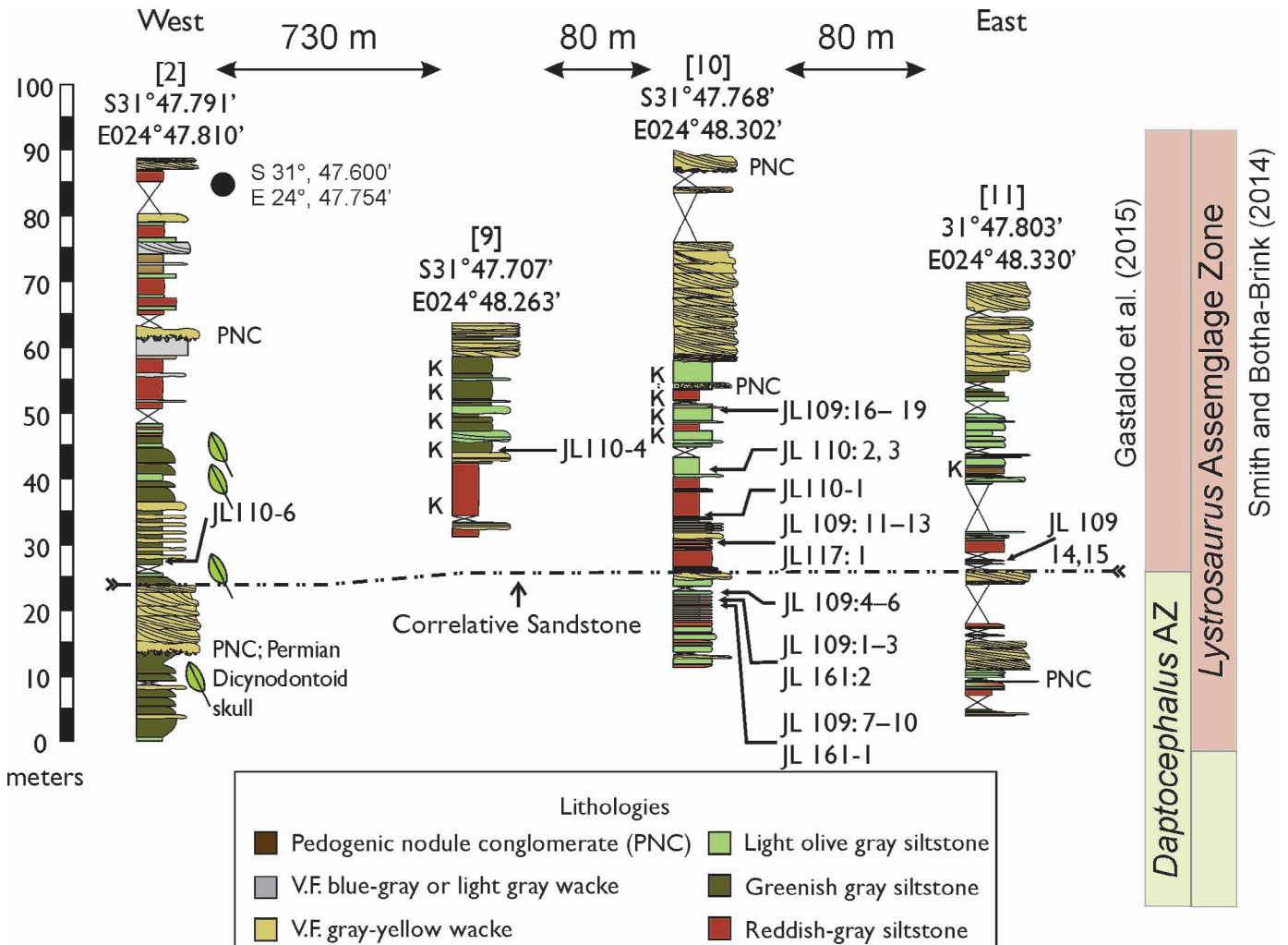


Fig. 3.—Collection sites of greenish-gray and reddish-gray siltstone in a correlative stratigraphic framework. The dashed-and-dotted datum is the upper bounding surface of the lithic wacke of Gastaldo et al. (2015), who place the boundary between the *Daptocephalus* and *Lystrosaurus* Assemblage Zones in this sandstone body. GPS coordinates mark the base of each section; GPS coordinates (WGS standard) of each sample are provided in Supplemental Data Table 1. GPS coordinates for the Old Lootsberg Pass section, as reported by Ward et al. (2000), corrected for longitude, appear as a solid black dot. K, *Katbergia* (Gastaldo and Rolerson 2008) burrowed siltstone intervals. Vertical scale in meters.

TABLE 1.—Mean concentrations of major elements (quantified as oxides) from XRF analyses of thin sections, and Mann-Whitney U Test results between greenish-gray and reddish-gray samples (statistically significant *p* values marked with *). Designations of (C) and (F) in samples JL109-13 and JL109-14 indicate analyses on coarse and fine intervals, respectively, of the thin section. All values reported in wt. %; standard errors in parentheses; samples numbers are in bold for greenish-gray siltstone.

Sample	Na ₂ O	MgO	Al ₂ O ₃	SiO ₂	P ₂ O ₅	SO ₃	K ₂ O	CaO	TiO ₂	MnO	FeO
<i>JL109-3B</i>	2.61 (0.02)	0.83 (0.01)	13.46 (0.05)	75.29 (0.07)	0.02 (0.01)	0.00 (0)	3.50 (0.02)	0.92 (0.01)	0.65 (0.01)	0.03 (0.00)	2.73 (0.01)
<i>JL109-8</i>	2.36 (0.03)	1.12 (0.01)	15.97 (0.07)	71.54 (0.13)	0.03 (0.01)	0.00 (0.00)	4.12 (0.03)	1.09 (0.02)	0.71 (0.02)	0.03 (0.00)	3.05 (0.03)
<i>JL109-10</i>	3.13 (0.05)	0.89 (0.02)	15.06 (0.10)	73.61 (0.18)	0.09 (0.02)	0.01 (0.00)	3.49 (0.04)	1.28 (0.04)	0.52 (0.03)	0.03 (0.00)	1.94 (0.03)
JL109-11	2.94 (0.04)	1.07 (0.02)	14.28 (0.11)	73.71 (0.19)	0.02 (0.00)	0.00 (0.00)	3.25 (0.04)	1.26 (0.02)	0.53 (0.01)	0.04 (0.00)	2.91 (0.05)
<i>JL109-13 (C)</i>	2.37 (0.08)	1.14 (0.03)	15.86 (0.20)	71.83 (0.35)	0.09 (0.04)	0.00 (0.00)	4.33 (0.08)	1.23 (0.05)	0.55 (0.02)	0.03 (0.00)	2.60 (0.08)
<i>JL109-13 (F)</i>	2.50 (0.07)	1.08 (0.03)	15.06 (0.13)	73.03 (0.24)	0.04 (0.01)	0.00 (0.00)	3.93 (0.06)	1.19 (0.03)	0.59 (0.03)	0.03 (0.00)	2.58 (0.08)
JL109-14 (C)	2.86 (0.05)	1.08 (0.02)	15.81 (0.10)	71.54 (0.18)	0.12 (0.03)	0.00 (0.00)	3.98 (0.04)	1.38 (0.04)	0.66 (0.02)	0.03 (0.00)	2.55 (0.03)
JL109-14 (F)	2.84 (0.04)	1.11 (0.02)	15.88 (0.08)	71.61 (0.14)	0.07 (0.02)	0.00 (0.00)	3.98 (0.03)	1.45 (0.03)	0.64 (0.02)	0.03 (0.00)	2.43 (0.02)
<i>JL109-15</i>	2.37 (0.04)	1.03 (0.02)	16.25 (0.10)	70.31 (0.18)	0.19 (0.03)	0.00 (0.00)	4.61 (0.04)	1.53 (0.04)	0.79 (0.02)	0.03 (0.00)	2.91 (0.04)
JL109-16	3.63 (0.06)	0.87 (0.02)	14.48 (0.11)	73.46 (0.20)	0.10 (0.02)	0.00 (0.00)	3.21 (0.05)	0.49 (0.03)	1.60 (0.06)	0.03 (0.00)	2.15 (0.04)
<i>JL109-18</i>	3.03 (0.04)	1.06 (0.02)	14.78 (0.08)	72.41 (0.15)	0.06 (0.01)	0.00 (0.00)	3.73 (0.04)	1.12 (0.02)	0.61 (0.02)	0.04 (0.00)	3.20 (0.03)
<i>JL110-1</i>	2.53 (0.04)	1.12 (0.01)	16.19 (0.08)	70.84 (0.15)	0.07 (0.02)	0.00 (0.00)	4.44 (0.04)	1.48 (0.03)	0.63 (0.03)	0.03 (0.00)	2.71 (0.03)
<i>JL110-2</i>	2.86 (0.06)	1.10 (0.02)	16.81 (0.11)	69.89 (0.19)	0.08 (0.02)	0.02 (0.01)	4.59 (0.05)	1.41 (0.04)	0.55 (0.03)	0.03 (0.00)	2.70 (0.05)
JL110-6	0.86 (0.05)	1.77 (0.03)	18.80 (0.12)	66.21 (0.19)	0.01 (0.00)	0.00 (0.00)	5.95 (0.05)	0.99 (0.02)	0.72 (0.02)	0.04 (0.00)	4.66 (0.05)
JL117-1	3.24 (0.06)	0.83 (0.02)	15.29 (0.12)	73.16 (0.21)	0.15 (0.04)	0.00 (0.00)	3.74 (0.05)	1.29 (0.06)	0.54 (0.02)	0.03 (0.00)	1.75 -0.04
Mann-Whitney U test between reddish-gray and greenish-gray samples N(greenish-gray) = 6 N(reddish-gray) = 9											
Z score	-1.24	0.18	0.29	-0.18	-0.06	-1.35	0.77	0.18	-0.53	-1.71	1.00
p value	0.21	0.86	0.77	0.86	0.95	0.17	0.44	0.86	0.60	0.09	0.32
U value	16	25	24	25	26	15	20	25	22	12	18
Critical U	10	10	10	10	10	10	10	10	10	10	10

samples from laterally correlative sites originate from sections 2 (N = 1), 9 (N = 1), and 11 (N = 2; Figs. 2, 3; Supplemental Data Table 1, see Supplemental Material). Seventeen of these samples were prepared as thin sections by Applied Petrographic Services, Inc., Greensburg, Pennsylvania. Polished hand samples supplement thin-section preparations.

Thin-section characterization included grain-size estimation, fining-up successions, and identification of sedimentary and biogenic structures. Grain size was estimated microscopically with NIS-Element BR 3.10 software, and digital images examined to determine dominant grain size and matrix content. Sedimentary structures were examined using a Nikon microscope and in polished hand samples (marked with “F” in Supplemental Data Table 1). Bedding style, the presence of mud chips and burrows, and the intensity of bioturbation were recorded.

Geochemical and Mineralogic Analyses

Geochemistry and mineralogy were characterized using three techniques. Bulk elemental composition was obtained using X-ray fluorescence (XRF), with multiple data acquisition points on each thin section or hand sample, whereas clay mineralogy was determined by X-ray diffraction (XRD). Because XRF data do not discriminate oxidized and reduced forms of Fe, selected samples were analyzed using Mössbauer spectroscopy (see Supplemental Data Table 1). Once the presence of finely dispersed hematite was confirmed by this technique, the distribution and morphology of hematite grains were assessed with scanning electron microscopy (SEM), and elemental composition was assessed with energy dispersive spectroscopy (EDS). Selected samples were analyzed for total organic carbon (TOC) with a PerkinElmer 2400 elemental analyzer. Details on methodology are provided in Supplemental Material.

Data on Rock Magnetism

Disaggregated samples were packed into appropriate nonmagnetic containers (either 7 cc IODP plastic boxes or size 04 gelatin capsules) for magnetic measurements. Measurements included bulk magnetic susceptibility (using an AGICO Kappabridge KLY-3S instrument), stepwise acquisition of an isothermal remanent magnetization (IRM) up to a field over 3.0 tesla (T), and backfield direct field demagnetization (using an ASC multi-coil impulse magnet with measurements on an AGICO JR5A spinner magnetometer), and determinations of magnetic hysteresis parameters using a Princeton Measurements Corporation vibrating-sample magnetometer (VSM). For determinations of the hysteresis parameters, small amounts (a few hundred milligrams) of disaggregated samples were mixed with Duco cement and then fragmented to make chips for VSM measurements. Finally, we monitored the bulk susceptibility of the samples as a function of heating to 640°C and subsequent cooling using an AGICO CS4 apparatus interfaced with an AGICO MFK1-A susceptibility system. These experiments were carried out in an argon atmosphere as well as in air.

Data Analyses

Descriptive statistics and bivariate plots (Sheldon and Tabor 2009) were constructed using XRF data. The Komolgorov-Smirnov test was run to determine which mean concentrations of major elements from greenish-gray and reddish-gray samples were distributed normally. Not all sample distributions conformed to a normal distribution. Hence, the Mann-Whitney U-test was used to compare elemental data between the two color suites. Pearson's Correlation Coefficient test was used to assess correlations between elements.

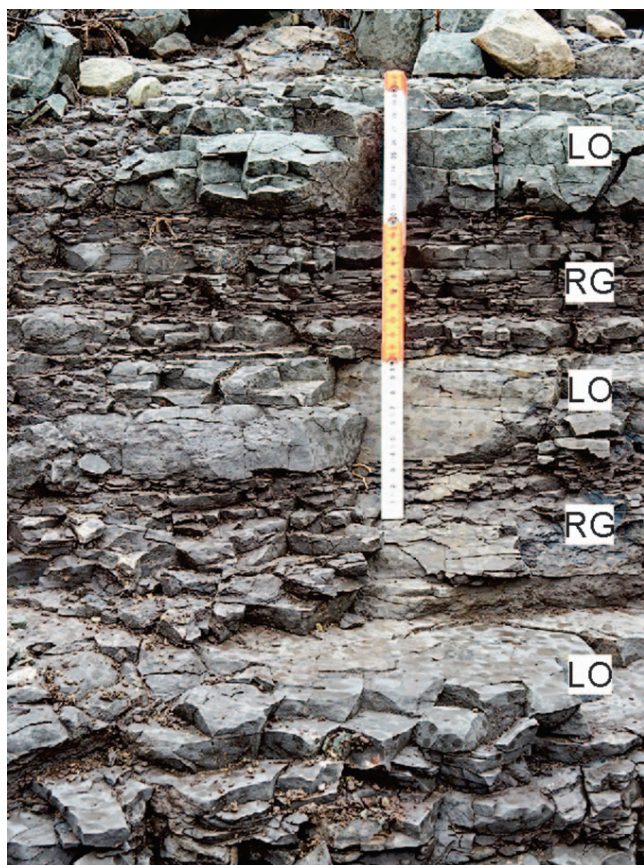


Fig. 4.—Interbedded greenish-gray and reddish-gray interval (S31° 47.74333', E024° 48.30750') in section 10 (Fig. 3) showing more resistant light olive (LO) coarse siltstone overlain by reddish-gray (RG) fine siltstone organized into planar and low-angle cross beds. Scale in decimeters.

RESULTS

The field characteristics of siltstone beds in the sampled interval vary in primary and secondary color, biogenic structures, and degree of weathering. Siltstone appears as either thick (> 30 cm) homogenous beds that are uniform in color, or intervals of interbedded, fining-upward successions wherein coarser and overlying finer beds differ in color (Fig. 4). Coarser siltstone commonly is greenish-gray and overlain by fine siltstone of a reddish-gray color. Although categorized in the literature as either olive-gray, gray, or maroon for the sake of convenience (Smith 1995; Smith and Ward 2001; Ward et al. 2000; Ward et al. 2005; Smith and Botha-Brink 2014), siltstone sample color varies greatly in each color suite (Supplemental Data Table 1). Greenish samples are distributed across several hues including greenish gray (Munsell hue of 10Y, 5BG or 5GY), olive to light olive gray (5Y 4/2-6/2), dark gray (5Y 4/1), or grayish brown (2.5Y 5/2). Samples with reddish coloration fall in the hues of dark to very dark gray (5YR 4/1-3/1, 10YR 4/1), dark reddish gray (10R 3/1-4/1), brown (7.5YR 4/2), gray (5YR 5/1), and dusky red (2.5YR 3/2). Hereafter, unless qualified for a specific sample, the terms greenish gray and dark reddish gray will be employed for each sample in each color spectrum. Mottling of these spectra is common. Primary structures include planar, lenticular, and low-angle cross beds, identified as a consequence of contacts between better and less well cemented beds (Fig. 4). Bedding ranges from millimeter- to centimeter-scale thickness, and erosional contacts are common. Small, spheroidal to ellipsoidal calcite-cemented concretions

(5–15 cm) are more common in reddish-gray siltstone intervals, and crosscutting *Katbergia* burrows (Gastaldo and Rolerson 2008) often are exposed for > 60 cm length. Isolated lenses of intraformational pedogenic nodule conglomerate (Pace et al. 2009) are present, albeit rare (e.g., S 31° 47.715', E024° 48.356'). Beds of coarse siltstone, regardless of color, generally are better cemented and more competent than intervals of fine siltstone. In most instances, less competent beds are weathered to a friable nature, clasts of which are transported downslope and cover exposure. This situation often imparts a false impression that a specific stratigraphic interval is dominated by one color or another and is massive in character. Thin sections of competent beds reveal a range of primary and secondary sedimentary structures in variously colored siltstone of these successions.

Greenish-Gray Siltstone

Petrographic examination shows that the presence of primary sedimentary structures is a consistent feature of greenish-gray siltstone (Figs. 5, 6). Fining-up intervals, ranging from 2 to 10 centimeters, of coarse to fine silt (Fig. 5A, C) may contain millimeter-sized mudclasts (Figs. 5D, 6C) as part of small, lenticular structures of the coarser fraction. Cross lamination, < 1 millimeter in thickness, fills ripple troughs with thin opaque (organic) drapes or micrometer-sized oxide grains that resemble organic-rich mud drapes defining bounding surfaces (Figs. 5C, 6C). Primary structures may be in sharp contact with underlying beds that are bioturbated, and exhibit an undulatory contact (Fig. 6B). Rarely are samples homogeneous in texture (Figs. 5B, 6A). In no instance, however, have clay drapes been observed. The Droser-Bottjer ichnofabric indices (I-I; Droser and Bottjer 1986) for these samples range from 1 to 5, with the highest category rarely encountered. In outcrop, burrows of *Katbergia* (Gastaldo and Rolerson 2008) are rarely encountered. Greenish-gray siltstone may be in direct contact with underlying or overlying dark reddish-gray siltstone (Fig. 7E), with a sharp boundary between colors. Similar primary structures characterize the other siltstone color suite.

Dark Reddish-Gray Siltstone

Dark reddish-gray siltstone exhibits a wider array of features than greenish-gray samples in thin section (Figs. 7, 8). Fining-up successions of coarse-to-fine siltstone in beds range from 2 to 5 millimeters in thickness, with internal structures either planar, rippled, or as low-angle cross lamination at the sub-millimeter scale (Figs. 7A, 8B, C). Color differentiation is stronger in the finer silt fraction. Beds of very fine sandstone with mudchip clasts, ranging from centimeters to decimeters in thickness, may be in erosional contact with intervals preserving primary sedimentary structures (Fig. 8B, C), and, in some instances, larger mudclasts may have inclusions of noncalcified spheroids (Fig. 7D). Indicators of subaerial exposure are rare (Fig. 8A), although these features may be a consequence of bioturbation which is a common feature. Burrows are subvertical (Figs. 7B, E, 8C) or inclined (Fig. 8B), and range in diameter from ~ 1 to 3 millimeters. Clasts in burrow fills consist of very fine sand grains, millimeter-size mudclasts (Fig. 8A), and bedded silt (Fig. 8B), and were piped down from overlying sediment (Figs. 7B, 8B). Greenish-gray burrow fills may exhibit dark reddish-gray rinds (Fig. 7E). Rarely are bioturbated intervals homogenized (Figs. 7C, 8D). The Droser-Bottjer ichnofabric indices (Droser and Bottjer 1986) for these samples range from 2 to 5. In outcrop, *Katbergia* (Gastaldo and Rolerson 2008) burrows are encountered infrequently.

Elemental Composition

Data on elemental composition obtained using XRF from thin sections originate from sampling areas that are similar in grain size and amount of

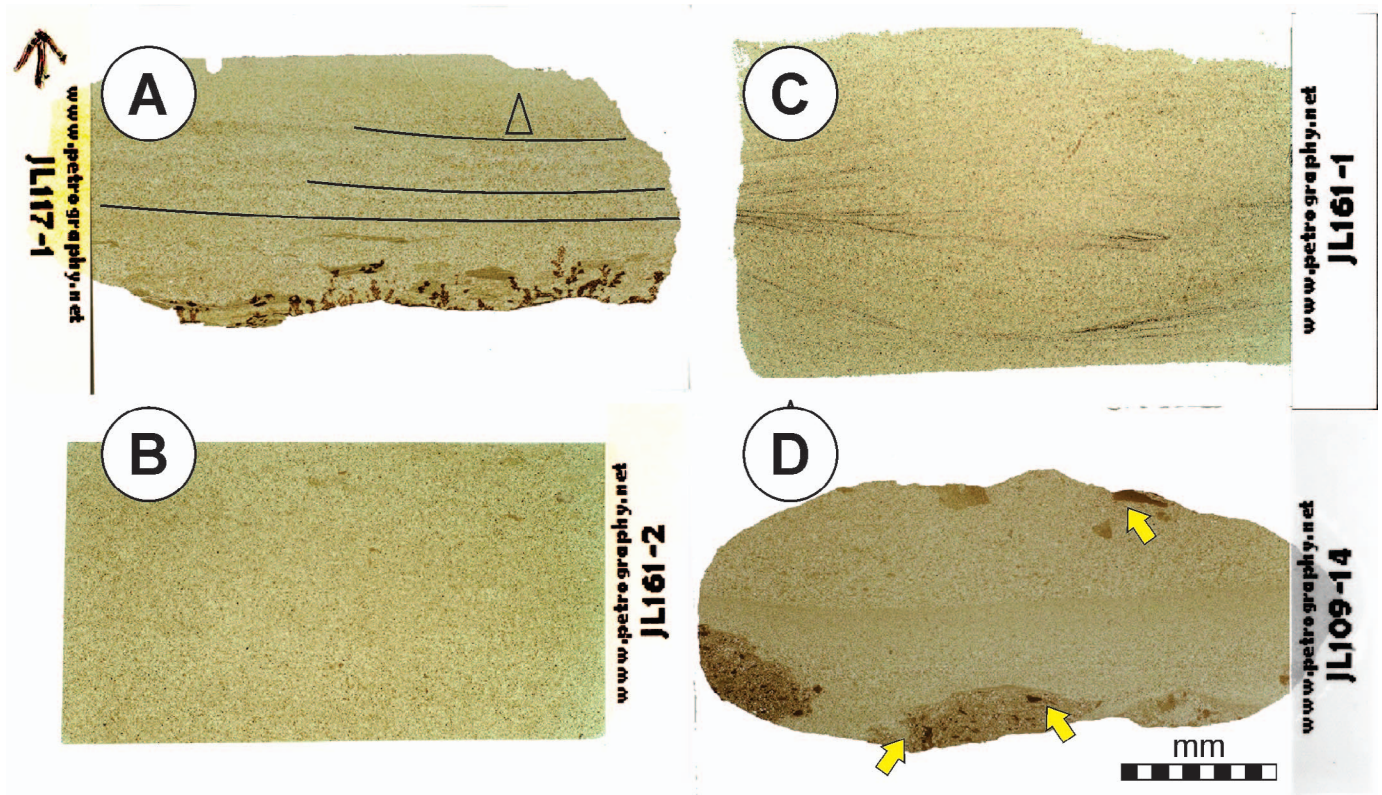


FIG. 5.—Thin-section photomicrographs of greenish-gray siltstones, the geochemistries of which all were analyzed with XRF (see Supplemental Data Table 1 and text). **A**) JL117-1, showing fining-up successions, the slightly undulatory upper surfaces of which are marked by black lines. **B**) JL161-2 is a thick bed in which faint, low-angle cross lamination occurs. **C**) JL161-1, exhibiting low-angle cross laminations, several accentuated by iron staining and/or organic drapes. **D**) JL109-14 shows coarse silt and very fine sand clasts with millimeter-size mudchips at the base and top (arrows). Scale in millimeters.

matrix. The mean concentration of all major elements in the greenish-gray and dark reddish-gray samples does not differ statistically (Table 1). Here, Si concentrations are high due to the abundance of quartz silt grains, and there is a strong linear correlation between Fe concentration and other major elements (Supplemental Data Table 2). Analysis of the clay fraction shows that only a few differences exist in the sample suite.

Data on mean elemental composition from the clay fraction of each sample overlap (Fig. 9), and most are statistically indistinguishable (Supplemental Data Table 3), with the expected result that the Si concentration is lower and the Al concentration is higher in comparison with “whole-rock” data obtained from the thin-section analyses. Greenish-gray and dark reddish-gray samples differ significantly in concentrations of Na, Ti, and Mn, and three dark reddish-gray samples (JL109-3, -4, -7) are outliers from the population defined by most samples (Fig. 9). There is a strong correlation only between Fe and both Si and Ti (Supplemental Data Table 3).

Clay Mineralogy

Despite the apparent color differences, all siltstone samples analyzed contain the same clay species (Table 2; Fig. 10). Ten peaks are present on the spectra obtained from KCl-treated slides with only three peaks, the 7 Å, 4.71 Å, and 3.53 Å, completely collapsed after being heated (Fig. 10B). MgCl₂ and Glycerol treatment did not have any visible effect on the spectra. Based on these data, only chlorite, illite, quartz, and feldspars are present at detectable abundance (> 1 wt.%; Table 2). No hematite peaks were observed across the spectra; this may be a function of the mineral’s low weight percent and detection limits of the XRD.

Oxidation State of Iron

Mössbauer spectroscopy provides quantitative data on concentrations of Fe²⁺ and Fe³⁺ in the sample suite (Table 3). All samples, regardless of color, have more than 50% of total Fe in the oxidized state. Dark reddish-gray samples have more Fe³⁺ than greenish-gray samples, and at least 15% of total Fe is in the form of dispersed fine-grained hematite. However, hematite is not restricted exclusively to dark reddish-gray siltstone, as it also is present in the olive-gray sample, JL109-16 (5Y 4/1), and represents about 7% of total Fe in this sample. The remaining olive-gray sample, JL109-10 (5Y 4/1), contains no detectable hematite (Table 3).

Iron-Oxide Morphology

The distribution and morphology of different oxide grains were examined qualitatively using SEM with species identification based on semiquantitative elemental compositions obtained via EDS. However, because X-ray scattering occurs on unpolished thin sections, data from surrounding minerals also were received by the instrument. Therefore, EDS data are considered only to be indicative of the mineral composition and cannot be regarded as unequivocal evidence for species identification.

Hematite crystals occur principally as coatings on clay minerals. The size of hematite coatings is highly variable, ranging from ~ 5 μm to as large as ~ 100 μm (Fig. 11), although sizes < 20 μm are most common. Hematite coatings are confined largely to illite, although coatings on chlorite are also present. Isolated hematite crystals and subequant grains are rare and, in general, small (~ 5 μm to ~ 20 μm). Hematite evaluated with EDS contains low Ti concentrations. Other opaque phases, such as ilmenite, rutile, and titanite, are present. Titanite and rutile also are found

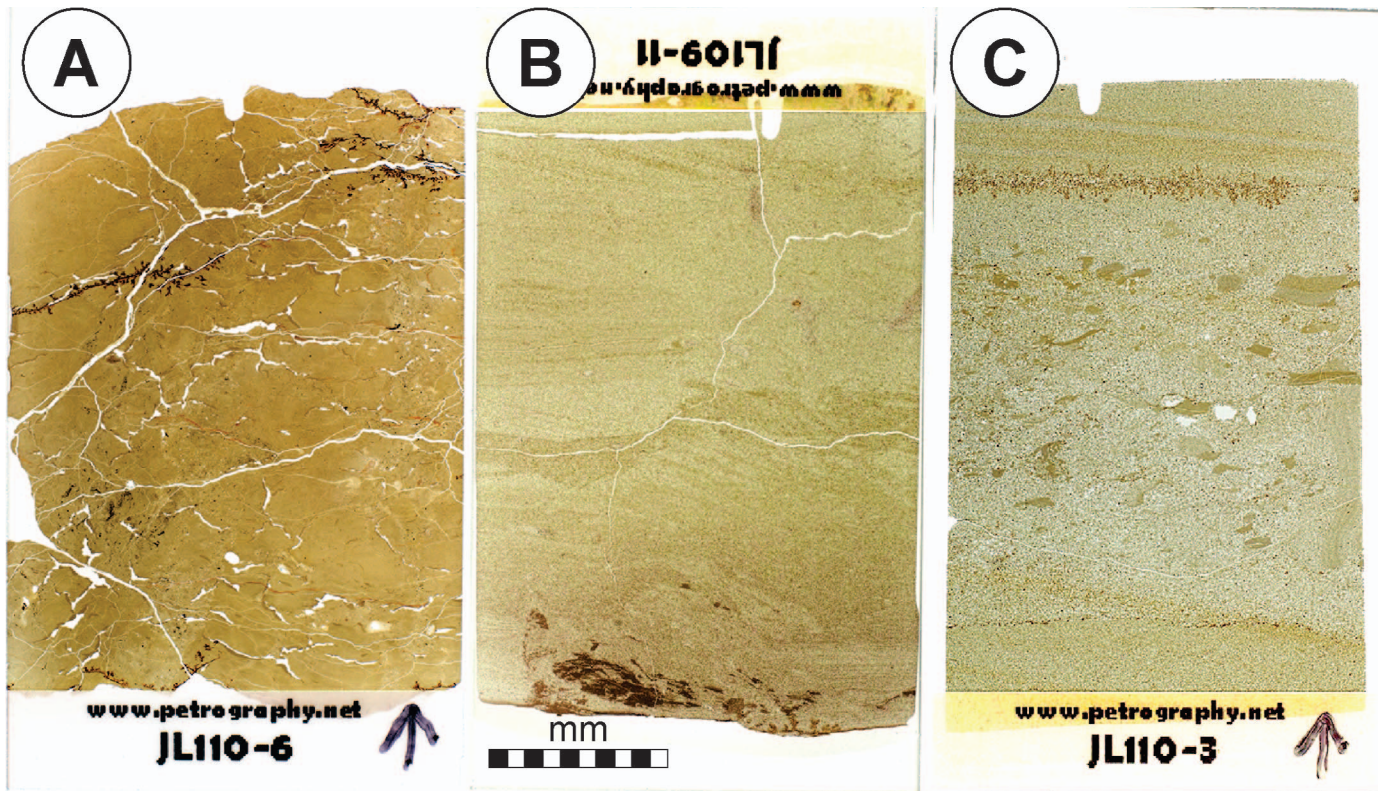


FIG. 6.—Thin-section photomicrographs of greenish-gray siltstones, the geochemistries of which all were analyzed with XRF (see Supplemental Data Table 1 and text). **A)** JL110-6, which appears homogenized by bioturbation. Note iron staining along cracks, which were avoided during XRF analyses. **B)** JL109-11 exhibiting bioturbated interval with a sharp, undulatory upper contact with siltstone in which low-angle, micro-cross lamination occurs. Mudchips are concentrated at the base of the section. **C)** JL110-3, showing homogenized interval in which millimeter-scale mudclasts occur, overlain by low-angle micro-cross lamination. Note iron staining along upper contact, which was avoided during XRF analyses. Scale in millimeters.

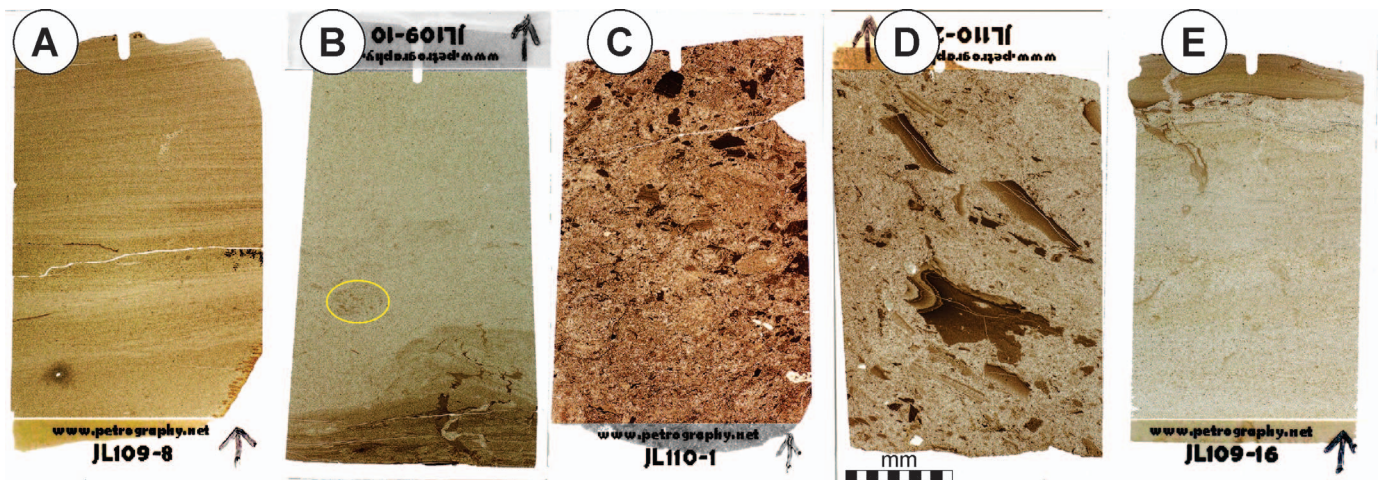


FIG. 7.—Thin-section photomicrographs of reddish-gray siltstones, the geochemistries of which all were analyzed with XRF (see Supplemental Data Table 1 and text). **A)** JL109-8, in which low-angle, fining-up successions of coarse-to-fine siltstone, several of which are at the sub-millimeter scale, and exhibit lenticular geometries, are preserved. **B)** JL109-10, wherein low-angle, micro-cross lamination is in sharp contact with overlying greenish-gray siltstone in which some color alteration appears surrounding mudchips and a compressed, vertical burrow. **C)** JL110-1 is a coarse, homogenized siltstone with millimeter-scale mudclasts and is bioturbated. **D)** JL110-2 is a coarse siltstone in which laminated and contorted mudclasts with noncalcified, spheroidal inclusions occur. **E)** JL109-16, showing fining-up successions in a greenish-gray siltstone in sharp contact with overlying, sub-millimeter-scale laminated reddish-gray fine siltstone that has been penetrated by a vertical burrow. The greenish-gray burrow fill is outlined by reddish-gray color. The upper contact is undulatory, and small mudchips are present. Scale in millimeters.

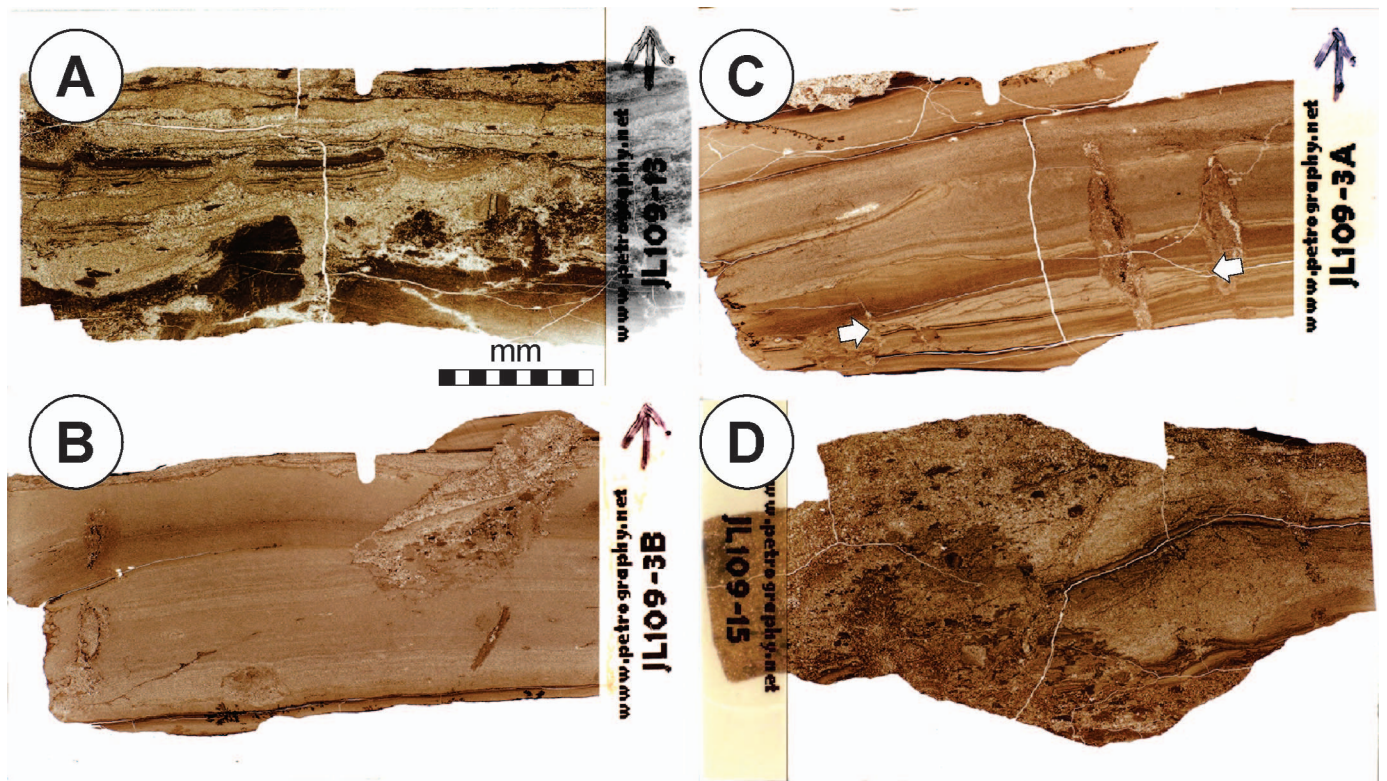


FIG. 8.—Thin-section photomicrographs of reddish-gray siltstones, the geochemistries of which all were analyzed with XRF (see Supplemental Data Table 1 and text). **A)** JL109-13, in which coarse silt and very fine sand grains (light-colored beds) are overlain by sub-millimeter-scale lamination and disrupted, either as a function either of short-term, subaerial exposure or bioturbation. **B)** JL109-3B, showing low-angle, sub-millimeter-scale lamination in sharp contact with a crosscutting inclined burrow. The burrow fill contains millimeter-scale mudclasts at the base, laminated mudclasts, and disorganized sediment. **C)** JL109-3A, in which millimeter-scale, fining-up successions of coarse-to-fine siltstone and a ripple (arrows) consisting of coarse silt grains occur. Coarse silt and very fine sand grains, along with mudchips, are in sharp contact with fine silt at the top, and probably represent a burrow fill. Two vertical burrows crosscut lamination. **D)** JL109-15, in which coarse silt and very fine sand grains are homogenized by bioturbation. Millimeter-scale mudclasts are scattered, and an inclined millimeter-scale burrow crosscuts the thin section. Scale in millimeters.

as coatings on illite, and ilmenite is more often identified as individual detrital grains. Both titanite and rutile were found in the more reddish-brown areas of the olive-gray sample, JL109-16 (Fig. 7E). Magnetite is identified in studies of rock magnetism (below), but SEM observations indicate that it is uncommon when compared to other oxides.

Bulk Magnetic Properties

Curves showing the acquisition of isothermal remanent magnetization (IRM) for all samples, regardless of color, are all concave downward and

show a rapid increase in IRM to saturation or near saturation below about 1.0 T (Fig. 12). Backfield demagnetization curves yield coercivity of remanence values that are consistently less than 300 mT. Hysteresis measurements show a variable range of hysteresis behavior, with coercivities ranging from 6.6 to 25 mT and squareness ratios (M_r/M_s) ranging from 0.014 to 0.090 (Fig. 13). Measurements of bulk susceptibility as a function of heating and cooling show that all materials yield distinctly irreversible curves, with increases in bulk susceptibility upon cooling that range from about 50 to over 250 percent (Fig. 14). All samples from both greenish-gray and dark reddish-gray siltstone yield heating-cooling curves that define, to varying degrees, the presence of a magnetic phase with Curie temperature of about 570 to 580°C, which we interpret to be magnetite. Several samples (e.g., 109-13, 110-2, 161-1, 161-2) show a decrease in susceptibility slightly above 300°C in the heating curve, and the absence of this behavior in the cooling curve.

TABLE 2.—Clay mineralogy of samples analyzed using XRD; representative spectra in Figure 10. See Methods for details.

Peaks Present	Identification
14 Å	Chlorite (primary)
10 Å	Illite (primary)
7 Å	Chlorite (secondary)
5 Å	Illite (secondary)
4.71 Å	Chlorite
4.5 Å	Yet to be identified
4.26 Å	Quartz (secondary)
3.53 Å	Chlorite
3.345 Å	Quartz (primary)
3.195 Å	Plagioclase

DISCUSSION

The relationships between siltstone color and geochemistry have a long history of investigation (Robb 1949; Keller 1953), with their application as a climate proxy in terrestrial rocks being an outgrowth of ideas about changes in iron oxidation states as a function of redox conditions. Greenish-gray mudrock has been used as a proxy for a prevailing wet (moist) climate at the time of deposition, whereas the presence of reddish-tinged mudrock has been thought to indicate a prevailing seasonally dry climate (e.g., Parrish 1998). Although the presence, alone, of reddened mudrock is shown not to be a proxy for climate (Dubiel and Smoot 1994;

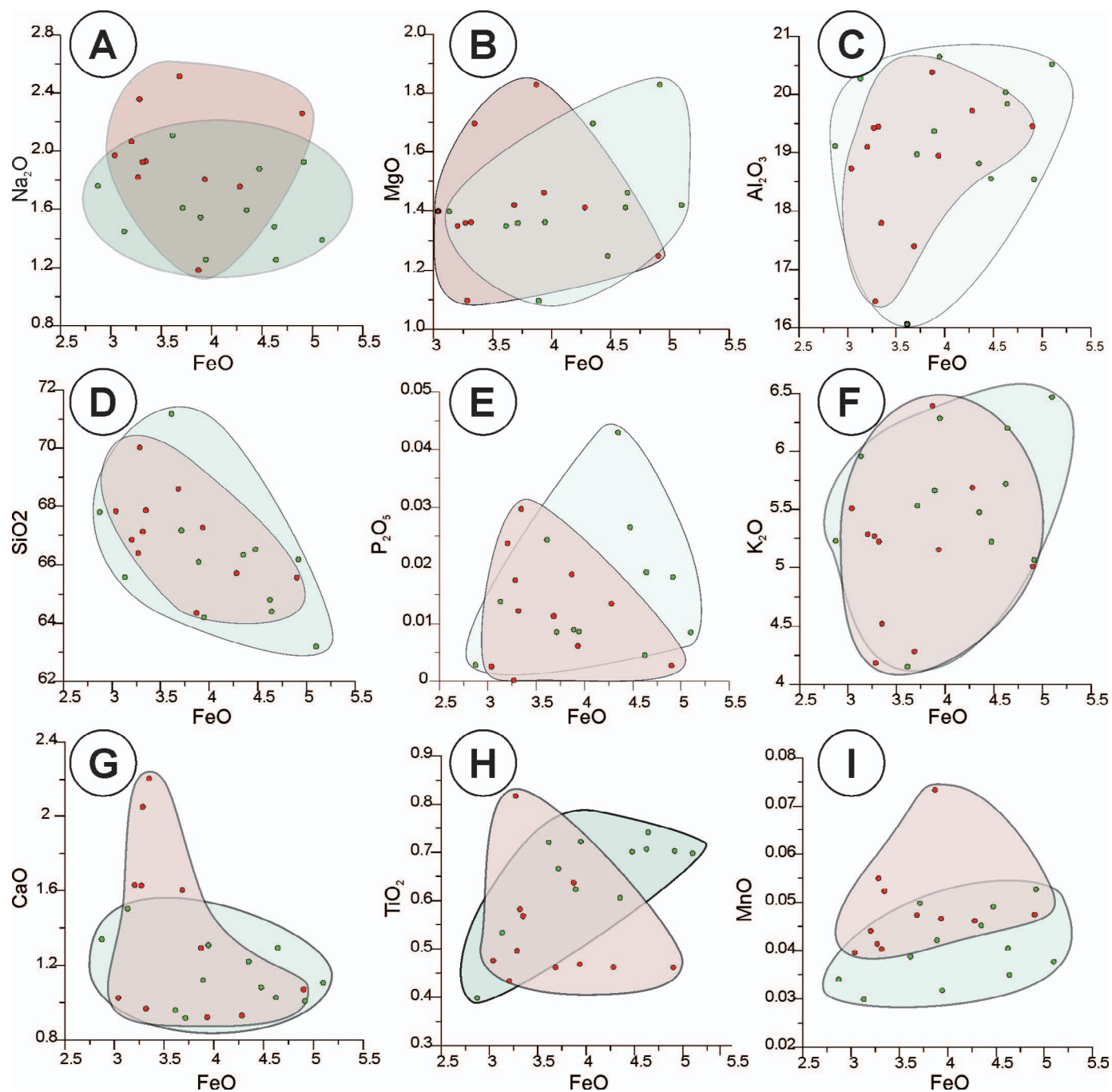


FIG. 9.—Bivariate plots of XRF mean elemental values in percent obtained from analyses of the clay fraction of greenish-gray (green circles) and reddish-gray (red circles) siltstones showing data-cloud overlap. **A)** FeO vs. Na_2O . **B)** Fe vs. MgO . **C)** Fe vs. Al_2O_3 . **D)** FeO vs. SiO_2 . **E)** FeO vs. P_2O_5 . **F)** FeO vs. K_2O . **G)** FeO vs. CaO . **H)** FeO vs. TiO_2 . **I)** FeO vs. MnO .

TABLE 3.—Results of Mössbauer spectroscopy of greenish-gray and reddish-gray samples. Values reported as percentage of total iron concentration. See Methods and Supplemental Material for details.

Sample Number	Color	Total Fe2+ %	Total Fe3+ %	Fe3+ in Octahedral Sites	Fe+3 as Fine-Grained Hematite	Hematite Concentration wt. %
JL109-3B	reddish-gray (5YR 3/1)	31.08	68.93	40.36	28.57	1.03
JL109-10	greenish-gray (5Y 4/1)	44.31	55.69	55.69	0	0.00
JL109-16	greenish-gray (5Y 4/1)	47.55	52.446	45.33	7.116	0.26
JL109-18	reddish-gray (5YR 3/1)	41.6	58.4	42.49	15.91	0.78

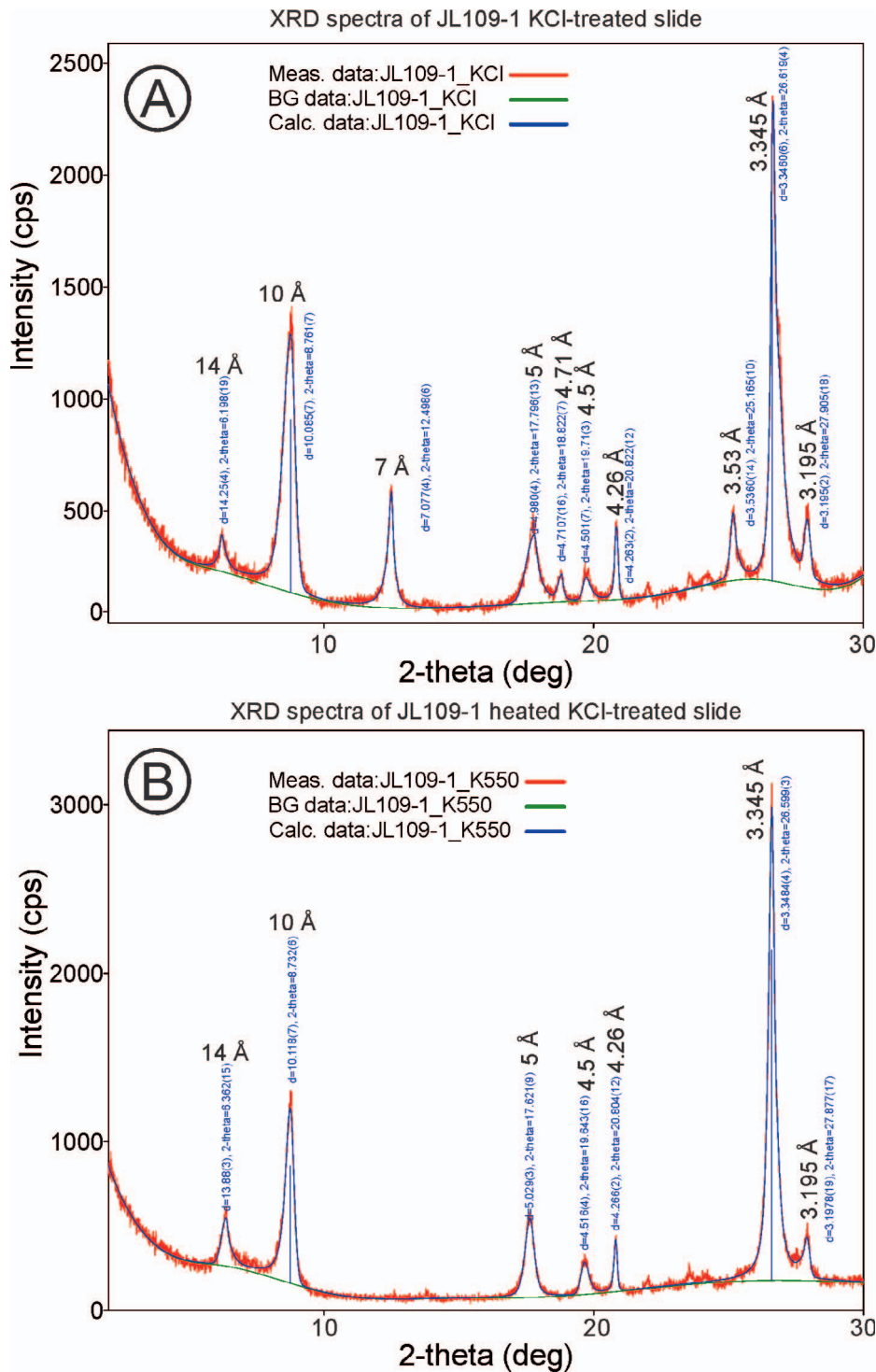


FIG. 10.—Clay-fraction XRD spectra of greenish-gray siltstone sample JL109-1. **A)** KCl-treated slide. **B)** Heated KCl-treated slide. Approximate *d* spacing used for identification of minerals labeled above or adjacent to peaks. XRD spectra obtained from chemically treated slides of all other samples display the same pattern.

Sheldon 2005), such an approach has been, and continues to be, taken in the interpretation of siltstone successions in the Karoo Basin transitioning the *Daptocephalus* (formerly *Dicynodon*; Viglietti et al. 2016) and *Lystrosaurus* Assemblage Zones (but see Gastaldo and Neveling 2016). Here, greenish-gray siltstone dominates the upper *Daptocephalus* AZ, and is interpreted in the literature to reflect sedimentation associated with a wet climate in which meandering river channels traversed floodplains (Smith and Ward 2001; Ward et al. 2000; Ward et al. 2005; Smith and Botha-Brink 2014) with high water tables (Gastaldo et al. 2014). An increasing

proportion of gray and maroon mottled siltstone in the uppermost *Daptocephalus* AZ (Smith and Botha-Brink 2014), followed by a transition to reportedly massive, uniformly reddened siltstone in the *Lystrosaurus* AZ (Fig. 3), is interpreted to be a function of aridification and drought (e.g., Smith and Ward 2001; Ward et al. 2005). The reported change in fluvial architectural style to an anabranching regime accompanies the color change (Ward et al. 2000). Smith and Botha-Brink (2014, p. 105) assert that the oxidation state of iron, responsible for the lighter maroon, dark red, and dark reddish brown coloration, is primary and a function of

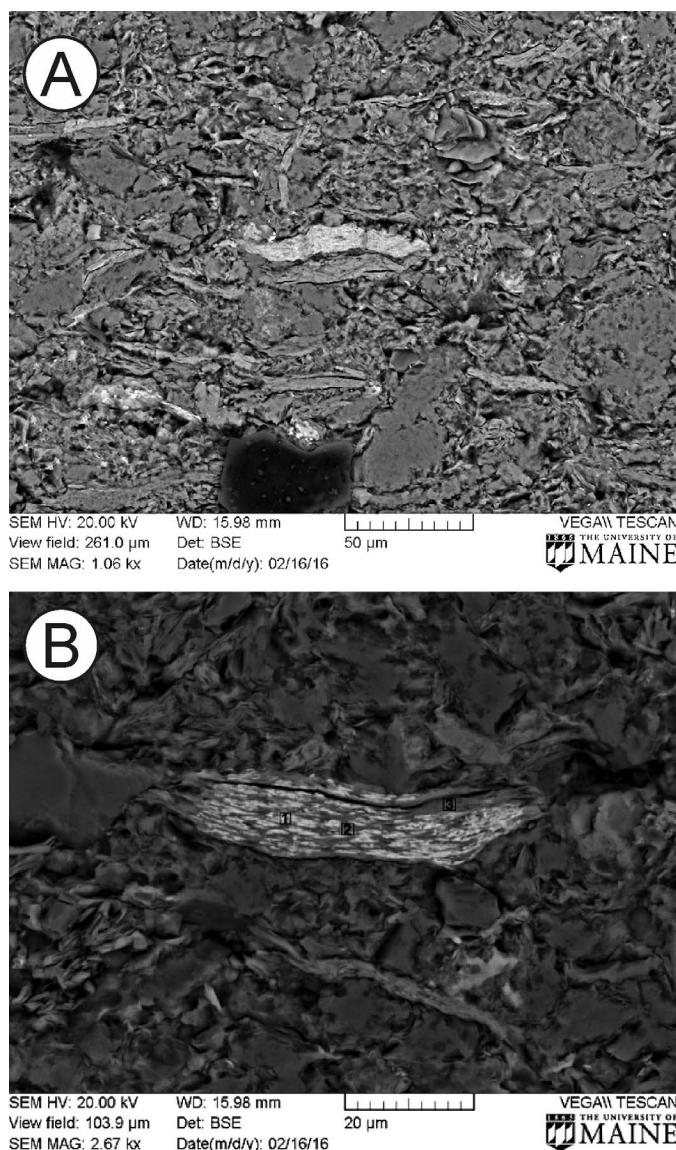


FIG. 11.—SEM images of hematite morphologies found on JL109-18 (see Supplemental Data Table 1). **A**) Hematite coating on clay mineral showing nearly complete coverage. **B**) Chlorite grain coated in a reticulated hematite; EDS data confirming iron oxide and clay composition obtained from points on clay labeled 1 and 2, respectively. Scale in micrometers as shown.

pedogenesis. They interpret these features to be the result of increased eolian contribution of fine iron oxide (i.e., magnetite, maghemite, and/or hematite) particles onto a dry floodplain, which, subsequently, were remobilized into the soil during periods of intense, wet seasonality associated with a monsoonal climate (Smith and Botha 2005; Botha and Smith 2006). Several studies of young loess sequences have demonstrated that it is common for enhancement of fine, superparamagnetic and single-domain magnetite to take place during pedogenesis (e.g., Evans and Heller 2001), and it is possible that the dark reddish-gray siltstone intervals of a range of hues may have magnetic properties very different from those of greenish-gray siltstone intervals. The results of our study demonstrate that a wide array of color variation exists in rocks having a surprising mineralogical and geochemical uniformity, in which both primary sedimentary and biogenic structures are preserved. In addition, we find no clear, distinct differences in magnetic properties between the siltstone

beds of different color. These results prompt questions about the mechanism of color alteration and the validity of previous interpretations regarding the depositional environment and climate ascribed to Karoo siltstone successions bounding the vertebrate-defined Permian–Triassic boundary event.

Variations in Siltstone Color

Considerable color differences exist in each suite of siltstone samples (Supplemental Data Table 1). Smith and Botha-Brink (2014) report the presence of gray mudrock as characteristic of the upper *Daptocephalus* AZ, although previous characterizations of these latest Permian paleosols range from greenish-gray (Smith 1995; Bada [Munsell 5 GY]; Retallack et al. 2003) to blue-gray, purple-gray, or dark reddish-gray hues (Bada [5B], Pawa, and Zam [10R]; Retallack et al. 2003; see Gastaldo et al. 2014, for a more complete assessment of these rocks). We find that siltstone beds at Old Lootsberg Pass are mainly greenish-gray in color, with Munsell hues ranging from 5Y, 10Y, and 10GY to 5BG. Other workers (Ward et al. 2000; Ward et al. 2005; Smith and Ward 2001; Smith and Botha 2005) have described the reddish-colored siltstone beds in the uppermost *Daptocephalus* and overlying *Lystrosaurus* AZs as “maroon” or “rubified.” Smith and Botha-Brink (2014) report that these generic colors correspond to dark reddish brown (2.5YR 2.5/4) for maroon mudrocks in their “event bed” (but see Gastaldo et al. 2009; Gastaldo and Neveling 2012; Neveling et al. 2016), and dark red (2.5YR 3/6) for earliest Triassic mudrocks. Only one of our samples exhibits the same hue (JL110-1, Table 1) whereas most are more appropriately described as hues of dark gray (5YR) and reddish-gray (10R) and “duller,” with a stronger grayish hue than “maroon.” When compared with color variants in other upper Permian rocks, the Karoo siltstone colors are muted. Variation in these siltstone colors can be explained by varying concentrations of fine-grained hematite and other brown-colored minerals.

Clay Mineralogy, Geochemistry, Rock Magnetism, and Siltstone Color

To date, the only clay minerals present at Old Lootsberg Pass and reported elsewhere in this stratigraphic interval are illite and chlorite (Pace et al. 2009; Gastaldo et al. 2014). This uniformity of clay mineralogy, regardless of color, indicates that greenish-gray colors are primary, while the dark reddish-gray colors are of diagenetic origin (see below). As indicated by the height of the primary peaks in the XRD spectra (Fig. 10A), illite is likely to be consistently higher in abundance than chlorite. Similarly, major-element concentrations in these rocks are uniform regardless of their color.

Elemental data from Old Lootsberg Pass are consistent with those reported from siltstone beds collected at Old Wapadsberg Pass, ~18 km to the southeast traced along and exposed below the same sandstone escarpment over the same stratigraphic interval (Fig. 1). Coney et al. (2007) processed greenish-gray and dark reddish-gray siltstone, beginning 7 m below to 7.5 m above the assumed vertebrate-defined boundary (see Smith and Botha-Brink 2014, their fig. 3). Although Coney et al. (2007, their fig. 3) only reported generalized sample colors in their section, preventing any statistical test of their data to demonstrate uniformity between greenish-gray and dark reddish-gray siltstones, they did not report any geochemical differences in the rocks. Rather, they do report an increasing trend in total Fe concentration up-section, with the maximum concentration (7.84 wt. %) immediately above the purported boundary. They interpret this trend as a response to a change in climate state towards aridification and, hence, iron enrichment. However, these authors were unable to duplicate this trend across the same boundary succession at either Commando Drift Dam, Eastern Cape Province, or Injustiti, Kwazulu Natal Province (Coney et al. 2007). Differences in elemental concentrations between their study and our current work, which also transitions the

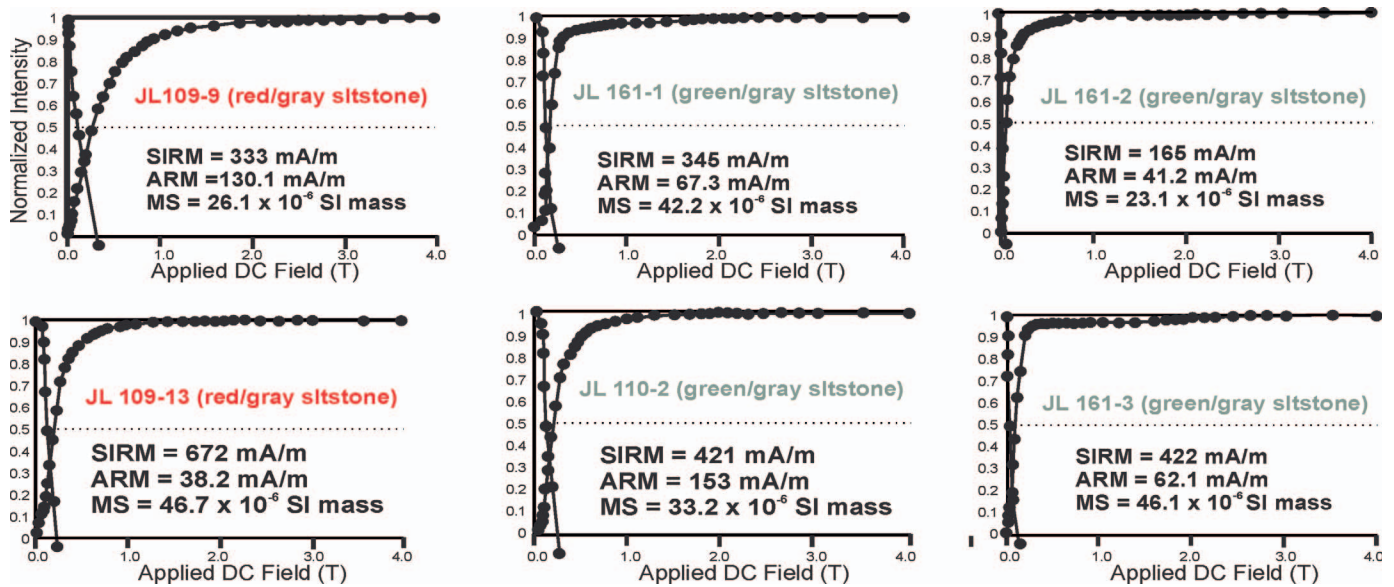


Fig. 12.—Curves showing the acquisition of an isothermal remanent magnetization (IRM) to saturation and backfield DC demagnetization for a powdered split of each of the samples analyzed and packed in a # 04 size gel cap for measurements. Values for saturation IRM (SIRM), anhysteretic remanent magnetization (ARM; acquired in a biasing DC field of 0.1 mT and a peak alternating field of 100 mT), and bulk susceptibility (MS) are indicated for each sample.

assemblage-zone boundary (Fig. 3) and demonstrates no trend or statistical difference in elemental concentration between different colored siltstones, may be a function of the analytical methods employed.

Coney et al. (2007) prepared thin sections of their samples and examined these optically to attempt to identify deformed quartz grains to examine the viability of an impact hypothesis that had been proposed for the extinction event, and supported by the findings of chondritic meteorite fragments in PTB strata in Antarctica (Basu et al. 2003). Unfortunately, they do not report whether the thin sections studied exhibit features of paleosols, as interpreted by Retallack et al. (2003), or primary sedimentary structures, which would be indicative of another depositional environment (see below). Rather, each whole-rock sample was powdered and a sample > 10 g was analyzed by XRF; the number of data-sampling points per sample is not reported. Hence, our sampling strategy of data collection from site-specific areas in each thin section, along with data collection from only the clay fraction of each sample, can account for the differences in elemental concentration between the two data sets. Al and K concentrations in siltstone beds from Old Lootsberg Pass are higher than those from Wapadsberg Pass, which is a reflection of the abundance of clay minerals in these rocks. Hence, the abundance of Si-rich silt grains present in whole-rock powders can disguise variations identified when only the clay fraction is analyzed. When quartz silt is present, the concentration of silica in the bulk analysis will be elevated. Similarly, the increasing trend in Fe concentration reported by Coney et al. (2007) may be an artifact resulting from the analysis of homogenized framework-and-matrix grains in their powders, incorporating secondary iron oxyhydroxides that were precipitated along weathered surfaces (e.g., Fig. 6C). Our data also indicate that the size and composition of grains included in any analysis of elemental concentrations can significantly influence correlations between elements. Strong correlations found in our data derived from whole-rock samples disappear once the silt grains of uniform mineralogy are eliminated and only the clay fraction is analyzed (Supplemental Data Tables 2, 3).

Retallack et al. (2003) characterized all siltstone intervals spanning a 40-m stratigraphic distance across the vertebrate-defined PTB at Carlton Heights, Lootsberg Pass, and Bethulie as paleosols, and reported major-element concentrations for three paleosol profiles. These are the greenish-

gray Bada soil type, assigned to the Permian, and a greenish-gray, weak red, reddish-brown Karie soil type and the Kuta soil type, reported to have the greatest variability in color from bluish-gray, reddish-gray, and greenish, assigned to the Triassic. Based on their published stratigraphic sections (Retallack et al. 2003 their fig. 4), the Karie and Kuta paleosols are in a stratigraphic position equivalent to that of our samples. Elemental data reported by Retallack et al. (2003) also are similar to our data from Old Lootsberg Pass, with observed differences only in Si and Fe (gross concentrations quantified as FeO) concentrations. Si concentrations in Retallack et al.'s (2003) paleosols are slightly lower (63.18–70.45 wt.%), while Fe concentrations are higher (3.77–6.78 wt.%, Fe_2O_3 converted to FeO), regardless of whether comparison is made with our data derived from analysis of thin sections or the clay fractions. Again, Retallack et al.'s (2003) reported higher concentration may be due to the presence of authigenic iron oxyhydroxide precipitates along fracture surfaces. Al concentrations are slightly higher in Retallack et al.'s (2003) paleosols when compared with values from our clay fraction. Silt grains in our samples are predominantly quartz, with a small feldspar (< 15%) component, whereas Retallack et al. (2003) report feldspar values of 25% in each rock analyzed. This compositional difference may explain the lower Si concentrations in paleosols when compared to those from our thin-section data, and higher Al concentrations when compared to the clay-fraction data. Where the siltstone and, hence, reported paleosol types, appear to differ is in the concentration of hematite.

Results from Mössbauer spectroscopy indicate the presence of finely dispersed hematite, in varying concentrations at < 1.10 wt %, that account for color differences between greenish-gray and dark reddish-gray siltstone. Hematite occurs as fine platelets, typically < 20 μm across and is found in both color suites. Two of four hematitic samples analyzed by Mössbauer spectroscopy are very dark gray in color, whereas a low percentage of fine-grained hematite occurs in an olive-gray sample (JL109-16; 5Y 4/1, Table 3). In sample JL109-16, the mineral is associated with a dark reddish-gray lining of a burrow that penetrated the underlying olive-gray siltstone (Fig. 7E). Samples with hematite have greater Fe^{3+} when compared to the samples without hematite (Table 3), which is a function of the mineral's presence for the coloration, per se. Greenish-gray siltstone with a much higher ferric Fe concentration than reddish-gray siltstone has

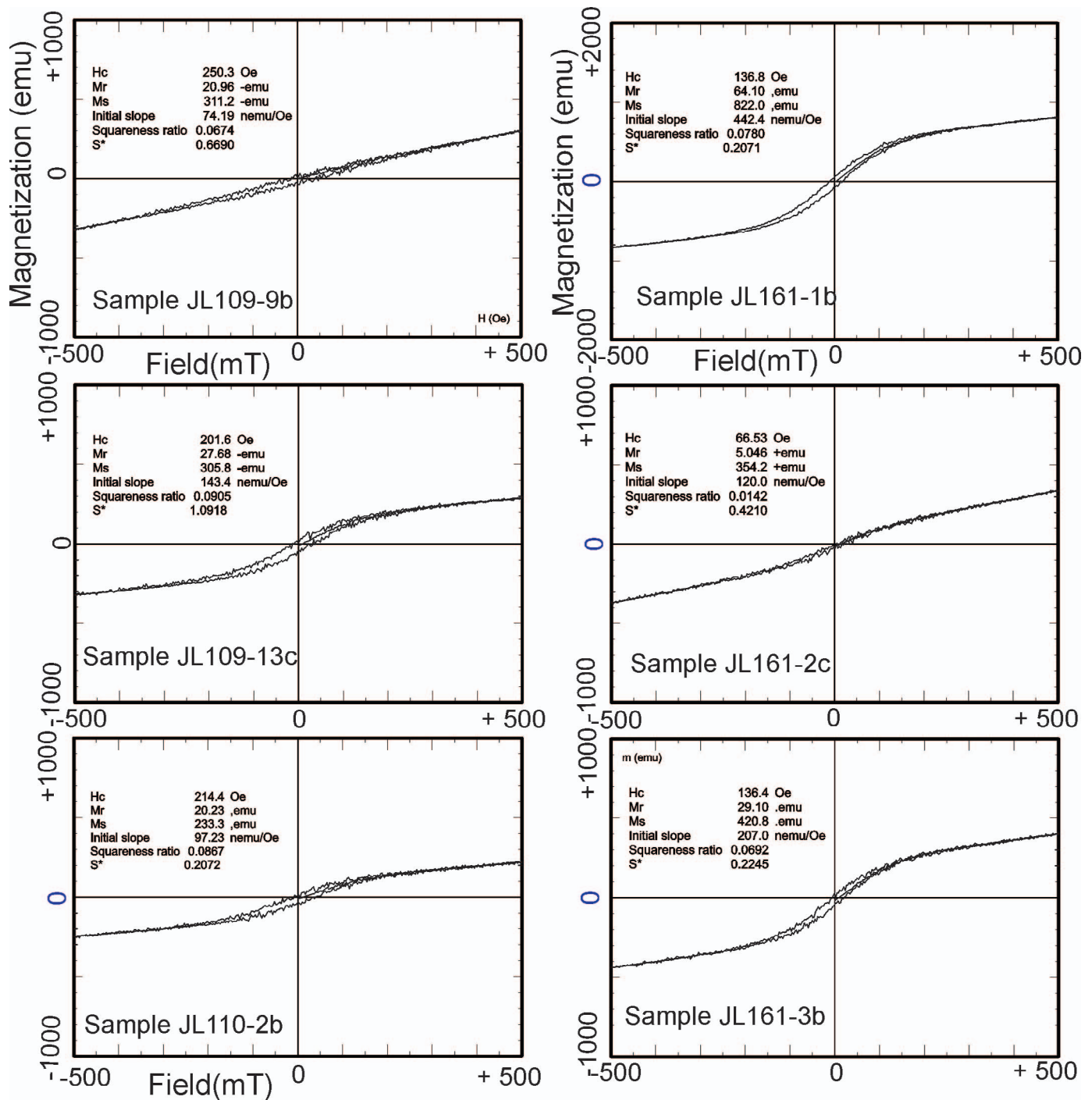


Fig. 13.—Magnetic-hysteresis curves and associated magnetic-hysteresis parameters. All curves were obtained with maximum DC field of (\pm) 500 mT.

been reported by previous researchers (e.g., Picard 1965). However, samples in which hematite is visibly more abundant do not necessarily have significantly higher total Fe values (Table 3). These results are interpreted to indicate that hematite content is not the result of contribution from external sources of Fe (e.g., hydrothermal fluids or eolian detritus; Smith and Botha-Brink 2014) over time. Instead, hematite likely formed from *in situ* alteration of pre-existing minerals; this is supported by the observed hematite morphologies and distribution of hematite as observed in SEM. Hematite is found most often as coatings on illite and chlorite

(Fig. 11), clays which may contain varying proportions of Fe (Murad and Wagner 1994; Johnston and Cardile 1987). Hence, iron in these clay minerals likely serves as a source for hematite formation, which is suggested by the mineral's reticulated pattern. In addition to hematite, silicate minerals including titanite and rutile may contribute to siltstone color.

Titanium oxide and other silicate minerals also are found in the dark reddish-gray siltstone beds. Rutile, titanite, and ilmenite are all strongly colored. Rutile typically is reddish-brown and black, whereas titanite is

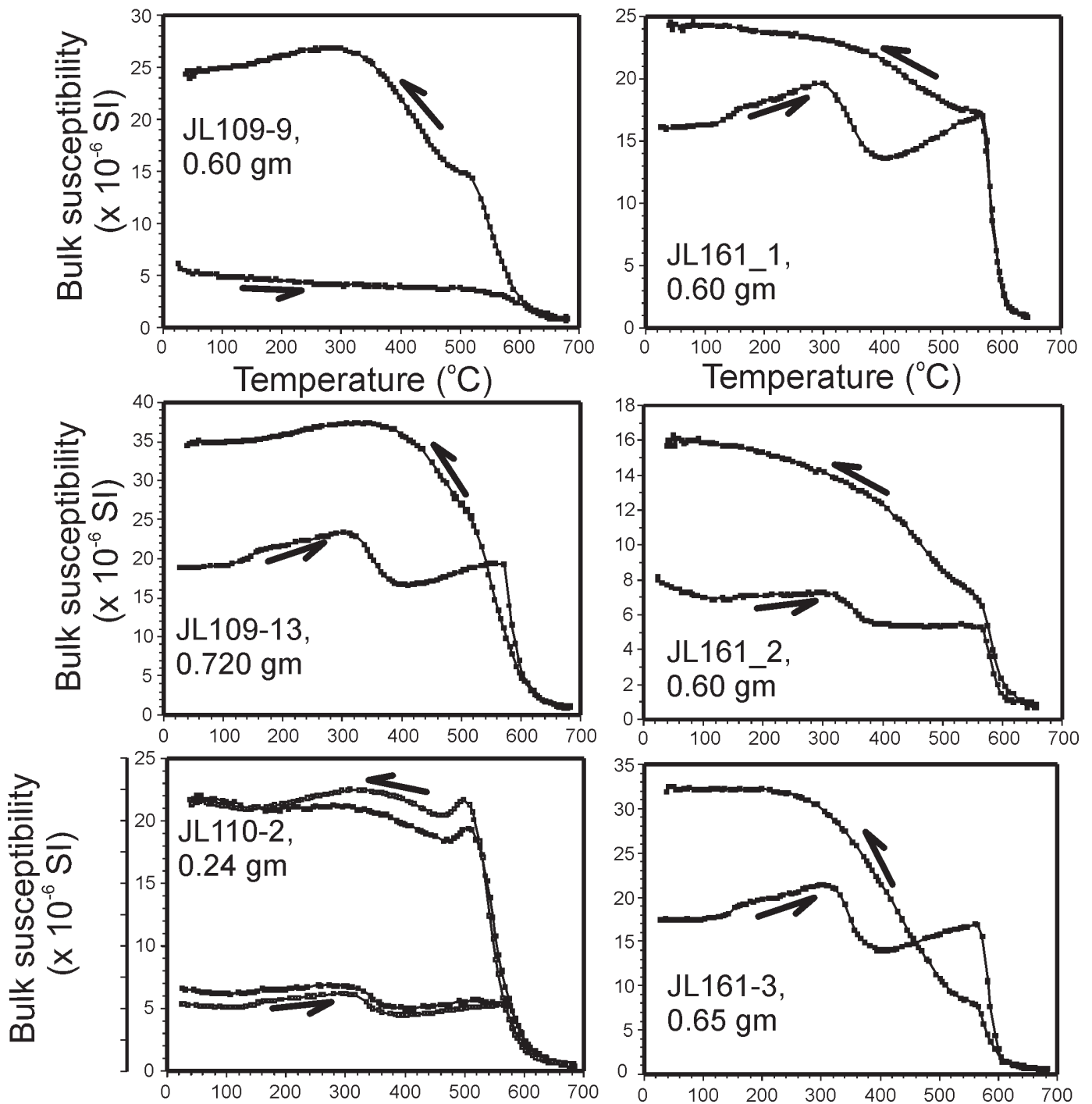


FIG. 14.—Plots showing the response of bulk magnetic susceptibility of powders of samples used in other rock-magnetism experiments as a function of heating and cooling in an inert (argon gas) atmosphere. Arrows show the heating (forward) and cooling (backward) curves. All curves are irreversible, with considerable increase in bulk susceptibility in cooling. Some samples (e.g., JL109-13, JL110-2, JL161-1, JL161-2, JL161-3) show a decrease in susceptibility slightly above 300 $^{\circ}\text{C}$, which we interpret as the conversion of maghemite to hematite. All heating curves demonstrate the presence of a phase with Curie temperature of about 580 $^{\circ}\text{C}$, which we interpret to be low-titanium magnetite. Note that two powder specimens from sample JL110-2 were run.

most often brown but can be red or black, as well (Nesse 2012). In contrast, ilmenite is only black in color (Nesse 2012). All three minerals are present in the most reddish-brown areas of thin sections (e.g., JL109-16), indicating that they may be responsible for either color enhancement or color variation in reddish-gray samples. Other workers also have reported Ti-rich minerals in reddish-gray and reddish-brown rocks (e.g., Picard

1965), but their influence on coloration has not received much attention in the past fifty years. The current results point to their potential importance in rock coloration, and future studies are needed to understand diagenetic enrichment of Ti-rich minerals and their relation to rock color.

The rock-magnetic data we have obtained on representative samples of greenish-gray and dark reddish-gray siltstone provide little evidence for a

clear distinction in magnetic mineralogy between the two lithologies. Rather, the data reveal considerable similarities in the two siltstone types. Curves of the acquisition of an IRM and backfield demagnetization of a saturation IRM show that all samples measured contain an abundance of a relatively low-coercivity, cubic phase that is likely a combination of magnetite and maghemite, in varying abundance. In comparison to other results, sample JL109-9 (of dark-gray siltstone) reaches complete saturation only above 2.0 T and shows the most distributed of IRM acquisition curves. These data demonstrate the presence of appreciable hematite, of higher coercivity. In contrast, sample JL161-3 (greenish-gray siltstone) shows a quick rise in IRM, implying relative low-coercivity cubic phases, and a notable increase in IRM over the peak field range of 1.5 to 2.1 (\pm) T, indicating the presence of measurable hematite. The squareness ratio obtained from hysteresis measurements of all samples indicates the relative abundance of coarse cubic magnetic phases. Results of bulk susceptibility versus temperature (heating and cooling in an inert, argon atmosphere) are perhaps the most revealing of the data sets. These data indicate that there is an appreciable increase in susceptibility after heating in all samples, implying the formation of new magnetic phases, likely additional magnetite. Heating curves for many of the samples show a distinct decrease in susceptibility over the temperature interval between about 310° and 380° C, which we interpret to demonstrate the conversion of some, if not virtually all, maghemite to hematite. In all cases, the cooling curves do not reveal an appreciable increase in susceptibility over this temperature interval. Notably, some samples of reddish-gray siltstone exhibit behavior very similar to those of greenish-gray siltstone (e.g., compare sample JL109-13 [dark reddish gray] with samples JL161-1 and JL161-3 [both greenish gray]; Fig. 14).

The stratigraphic sections at Old Lootsberg Pass are dominated by greenish-gray siltstone, with dark reddish-gray siltstone often exposed as its spatially related lateral equivalent (Fig. 3; Neveling et al. 2016; Gastaldo et al. 2017). Illite is reported to be the most abundant clay mineral in greenish-gray siltstone that lack hematite from many other localities (e.g., Robb 1949; Picard 1965; Thompson 1970), and the occurrence of chlorite also is partially responsible for their color (e.g., Thompson 1970). Therefore, the presence of these two clay minerals in the upper *Daptocephalus* and lower *Lystrosaurus* Assemblage Zones likely accounts for the initial (greenish-gray) siltstone color. Slight variation in their relative abundance may be responsible for differences seen in siltstone hues. Notably, dark reddish-gray siltstone has the same clay mineralogy, indicating that these rocks originally were greenish-gray in color, as well. Their modification is a result of early diagenesis, wherein some Fe in clay minerals was altered to hematite coatings, resulting in a dark reddish-gray color. Hence, the combination of lithostratigraphic relationships (Fig. 3), primary sedimentary structures (Figs. 5–8), and geochemical equivalence (Figs. 9, 10), indicate that greenish-gray and dark reddish-gray siltstones are lateral facies equivalents, with color alteration to the latter principally a function of fine-grained hematite precipitation on illite and chlorite clay-sized clasts.

Depositional Environment

All siltstone intervals in the upper *Daptocephalus* and lower *Lystrosaurus* Assemblage Zones, regardless of color, have been interpreted as an array of paleosol types (Smith 1995; Retallack et al. 2003; Smith and Botha–Brink 2014), whereas sandstone architectures represent deposition in one or more fluvial channel geometries (Smith and Ward 2001). Paleosols in siltstone from Lootsberg Pass (Fig. 1) generally are characterized as being of moderate thickness (Bada, 50–90 cm; Kuta, 40–70 cm; Karie, 40–100 cm; Retallack et al. 2003, data repository item 2003122) with relict bedding in some underlying sandstone intervals interpreted as a C horizon. Woody and thin (5 millimeter) root structures or traces are reported in the Bada type of the *Daptocephalus* Assemblage

Zone to extend for up to 76 cm depth accompanied by the presence of small nodules (< 12 cm diameter). In contrast, rooting in the Kuta soil type may be up to 1 cm in diameter with nodules attaining a maximum diameter of > 30 cm. Similarly, the Karie pedotype possesses rooting structures up to 95 cm depth, slickensides, small (< 5 cm) to large (< 23 cm) calcareous nodules, and *Katbergia* burrows. To date, siltstone successions overlying bedload deposits have not been interpreted as channel-fill accumulations in response to channel abandonment or avulsion.

The siltstone successions that we have measured, described, sampled, and characterized across the *Daptocephalus* to *Lystrosaurus* Assemblage Zones at Old Lootsberg Pass exhibit the same color spectrum as at other reported boundary sections in the Karoo, yet we observe only a few of the characteristics ascribed by Retallack et al. (2003) to their paleosol types. We find no evidence of preserved thick (1 cm) or thin (< 5 millimeter), deeply rooted intervals and only infrequent, horizons of calcite-cemented nodules in any of the several hundred meters of 11 correlated sections (Figs. 2, 3). Such features are present in paleosols at Wapadsberg Pass (Gastaldo et al. 2014) where stable isotope data indicate carbonate cements of these nodules precipitated in response to methanogenesis below the water table. We do record the presence of *Katbergia*-burrowed intervals upwards in our sampling interval, in greenish-gray, light olive-gray, and dark reddish-gray intervals at Old Lootsberg Pass. We also agree that these successions are probably paleosols, albeit ones formed under wet soil conditions (Gastaldo and Rolerson 2008; Pace et al. 2009), or exposed surfaces of in-channel barforms, rather than representing one or more soil types formed under a seasonally dry climate as is the model for the *Lystrosaurus* Assemblage Zone (Smith and Botha–Brink 2014; Viglietti et al. 2016). Outside of these *Katbergia*-burrowed intervals, there is no evidence in thin sections for clay skins, peds, or cutans, which would support pedogenic modification of the gray and maroon sediments (Retallack 2001). The evidence we report from thin sections in this study, and elsewhere, indicate a different depositional setting for siltstone underlying *Katbergia*-bearing paleosols.

Primary sedimentary structures that are consistent with formation by fluvial processes are the most common features of both greenish-gray and dark reddish-gray siltstone intervals. These include low-angle, micro-cross lamination (Fig. 5C) and ripples (Fig. 8C) of bedload origin, as well as thin successions of coarse-to-fine silt deposited from suspension load (Figs. 5A, 7A, E, 8B, C). These features are in stark contrast to primary structures associated with silt loams deposited via eolian processes where weakly developed, intercalated fine-sand-and-silt laminae form in simulated conditions under water (Mücher and de Ploey 1990). Most thin sections preserve evidence of small-scale bioturbation, where burrows are mostly inclined or vertical (Figs. 7B, E, 8B, C), or where the sediment has been homogenized (Figs. 6, 7C, D, 8A, D). In our sample suite, bioturbation is associated more often with dark reddish-gray siltstone. Burrow fills are composed of sediment originating from above the bed contact and include millimeter-scale mudclasts, which may appear “brecciated” (Retallack et al. 2003; Retallack 2005), very fine sand, and coarse silt which also show signs of suspension-load sedimentation. On occasion, burrows are lined with hematite (Fig. 7E). Hence, thin-section observations indicate that much of the stratigraphic successions that overlie thick to thin, lithic wacke architectural elements are consistent with those of fluvial origin and not supportive of either eolian or pedogenic processes operating in the lower *Lystrosaurus* AZ. This interpretation also is consistent with paleontologic data.

Gastaldo et al. (2015, 2017) document the occurrence of *Glossopteris* leaves in the *Lystrosaurus* AZ. Leaf impressions have been found at several stratigraphic horizons in greenish-gray siltstone that is laterally equivalent to both the greenish-gray and dark reddish-gray sampled intervals in section 10 (Fig. 3). The physiochemical conditions and depositional environments, or taphonomic windows, under which plant parts can be preserved across the possible terrestrial landscape settings are

well known (Behrensmeier et al. 2000; DiMichele and Gastaldo 2008). Although long-term changes in the subsurface position of the water table across a landscape, in response to Milanković-scale climate oscillation, may prevent soft-tissue preservation (Gastaldo and Demko 2011), the presence of *Glossopteris* leaves in section 2 (Fig. 3) is evidence in support of rapid burial at the sediment–water interface of a channel-fill succession (e.g., Gastaldo et al. 1989). Sufficient quantities of available water in the *Lystrosaurus* AZ landscape also are supported by the wood anatomy of *Agathoxylon africanum* close to the vertebrate biozone contact (Gastaldo et al. 2015; Gastaldo et al. 2017). The permineralized wood, with a diameter > 0.5 m, exhibits complacent growth rings (Gastaldo et al. 2017). These are a feature of woody trees that show a low degree of annual variation in any limiting growth factor (water availability, temperature range, nutrients, etc.).

Conditions Associated with Color Alteration

Siltstone color alteration under wet conditions, and in-channel fluvial settings, may be related to spatial and temporal variation in pre-burial hydrology. Redoximorphic features in paleosols are documented to be associated with changes in the hydrology across an original landscape before burial, which are ascribed to changes in soil chemistries as a function of saturation (e.g., Kraus 1997; Sheldon 2005; Kraus and Hasiotis 2006). Color variation, in turn, is controlled by interactions among bacteria, organic matter, and sediment over various temporal and spatial scales. The appearance of greenish-gray sediment, characterized by an absence of hematite, can be modified to a mottled appearance where localized pockets favor anaerobic conditions. Short-term anaerobic conditions promoting iron-and-manganese reduction, movement, and oxidation can be associated with the decay of organic matter, and would be represented by Fe oxide coatings or burrow linings. A change from gray to dark reddish paleosols, displaying redoximorphic concentration where mobile Fe and Mn are oxidized (Tabor and Montañez 2004), is demonstrated to be more a function of spatial and temporal variation in hydrological drainage rather than of increased seasonality (monsoonal) or desertification (Sheldon 2005). Preliminary examination of samples in the current study show that their TOC content (avg. 0.40%) is too low for organic matter to be the principal factor responsible for color alteration.

Other factors, such as changes in pH and/or Eh of water in the depositional setting (Keller 1953), may be related to hematite formation in sediments. Schwertmann et al. (1999) found that hematite formation is favored over goethite when the pH of freshwater is close to the zero-point charge of ferrihydrite, which is likely a function of its solubility minimum in this range. And, when organic acids are present, hematite formation also is promoted over goethite because ferrihydrite dissolution is slowed by blocking specific dissolution sites by ligand absorption (Baldock 2002). Under experimental conditions, illite becomes unstable and starts to dissolve when the ambient pH is < 4 or > 11 (Köhler et al. 2003). The dissolution of illite may release structurally-bound Fe, which, then, may be transformed into the more stable hematite by microbial processes (Velde and Meunier 2008). Hence, there are several mechanisms by which hematite may be precipitated in continental settings, and thin-bedded siltstone intervals of alternating colors may have resulted from periodic changes in pH and/or Eh of discharging channel waters or pore-water flux in floodplain sediments.

Benison et al. (2007) document the sedimentology of lake, mudflat, and sandflat facies surrounding ephemeral acid saline lakes in western Australia, where a mixture of siliciclastic and chemical sediments accumulates. Siliciclastic lake facies are characterized by planar lamination and cross lamination associated with thin beds, which may be rippled, that are disrupted by lateral and vertical “pipes” resulting from evaporite (halite, gypsum) dissolution. In contrast, primary structures found on sandflats and mudflats exhibit interference ripples, mudcracks, and

raindrop imprints, with little evidence of subsurface evaporite minerals and iron-oxide staining. Here, color modification is attributed to early diagenetic formation of iron oxides in the shallow subsurface. Although our samples exhibit a suite of primary sedimentary structures of similar nature, we find little physical evidence and no geochemical evidence in support of such an extreme depositional setting in this stratigraphic interval. Color alteration also is reported as a response to post-burial phenomena.

In a study of the Navajo Sandstone, Beitler et al. (2003) interpret variation in coloration between reddish and non-reddish hues to have been the result of early diagenetic flux in hydrocarbons. They postulate that regional bleaching phenomena altered an original reddish color of the sandstone as a consequence of variation in intraformational permeability relative to structural highs. As such, color alteration was in response to secondary hydrocarbons that migrated through coarser sediment, bleaching these beds. We find that both olive-gray and dark reddish-gray siltstone contain the same proportion of Fe, and color variation in these lithologies is not restricted to coarse versus fine-grained beds, respectively. Rather, coarse siltstone may be of either coloration, and laterally equivalent beds often grade from mottled to a uniform color (Neveling et al. 2016; Gastaldo et al. 2017). If early diagenetic hydrocarbon flux influenced siltstone coloration, we would expect to see the pattern exhibited over much larger areas, rather than restricted to distances of a few hundred meters (Fig. 3; Gastaldo et al. 2015; Neveling et al. 2016). And, although some siltstone intervals at Old Lootsberg Pass appear massive due to their uniform coloration, on close examination we find that unweathered rock is laminated with lateral equivalents of a different color within several hundred meters. Therefore, the uniform coloration of any siltstone interval is likely the result of late-stage, rather localized diagenesis, instead of primary color alteration before or during the early stages of burial.

Bioturbation also may locally promote hematite precipitation. Depositional successions in greenish-gray mudrock where there is little evidence for bioturbation show minimal hematite formation. Where this occurs, generally, is associated with iron-oxide precipitation along burrow margins in response to oxidation (Fig. 7E). In contrast, increasing dark reddening is associated with mudrock that experienced the greatest degree of biological mixing and hematite precipitation.

CONCLUSIONS

Coloration of Karoo siltstones has been used as evidence in support of a climate-change model to explain the turnover in vertebrate assemblage zones from the *Daptocephalus* to *Lystrosaurus* faunas (Ward et al. 2000; Smith and Ward 2001; Smith and Botha-Brink 2014; Viglietti et al. 2016). This turnover has been interpreted to represent the response of terrestrial ecosystems to the end-Permian crisis (Benton and Newell 2014; Rubidge et al. 2016). To date, all siltstone deposits in the Beaufort Group are presumed to be floodplain deposits and paleosols (Smith 1980, 1990, 1993, 1995), and their coloration is interpreted to be a function of iron oxidation state controlled by atmospheric conditions. However, such extensive use of the physical features of these rocks as climate indicators has not been tested either petrographically, mineralogically, or geochemically. Our data from correlative sections in the uppermost *Daptocephalus* and lower *Lystrosaurus* Assemblage Zones from Old Lootsberg Pass, encompassing ~ 700 m of measured stratigraphic section, indicate that the prevailing assumptions about these rocks require reinterpretation.

Both greenish-gray siltstone and dark reddish-gray siltstone preserve a suite of undisturbed to minimally disturbed primary structures. These include low-angle cross lamination, ripples, and fining-up successions, at the sub-millimeter and millimeter scale, that indicate deposition in a fluvial channel setting without periodic exposure to subaerial conditions or plant colonization and disruption by phytoturbation. No evidence is seen for pedogenic alteration of these rocks. The environment in which these

sediments were deposited shows signs of low-flow or quiet-water conditions, as bioturbation is associated with intervals in both colored rocks. Mixing features, including vertical and inclined burrows, range from Ichnological Indices of 1 to 5 (Droser and Bottjer 1986), wherein higher indices more often are associated with dark reddish-gray mudrock. *Katbergia* burrows (Gastaldo and Rolerson 2008) may be present, indicating that the area experienced variations in the level of the water table over time. These features are interpreted as channel-fill sequences in slackwater areas associated with late-stage channel fill.

Few statistical differences exist in the major-element composition of the two mudrock-color suites, which compare favorably with other geochemical data reported from the area (Retallack et al. 2003; Coney et al. 2007; Gastaldo et al. 2014). Differences found between the Old Lootsberg Pass data and these other datasets include the reported percentages of Si and Al in each study interval. These differences are a function of the methods used in sample preparation for XRF analysis. Differences in the proportion of Na, Ti, and Mn are likely a function of mineralogy. XRD data indicate the presence of only two clay minerals, illite and chlorite, which are consistent with other reports from the area (Pace et al. 2009; Gastaldo et al. 2014). The only significant difference between greenish-gray and dark reddish-gray siltstone is that the latter contains very low concentrations (< 1 wt.%) of hematite in the form of coatings on some clay-mineral grains, and not the proportion of Fe²⁺/Fe³⁺, per se. Hence, the mere abundance of Fe does not account for either color. Rather, illite and chlorite clasts not coated with hematite account for the greenish-gray color whereas variation in dark reddish-gray coloration is in response to an increasing proportion of finely dispersed hematite at low weight percentages. In addition, the presence of Ti-rich minerals (titanite, ilmenite, and rutile) may explain the color variation observed in the more reddened siltstones.

The recognition that greenish-gray and dark reddish-gray siltstone are unequivocally present at laterally equivalent stratigraphic positions at Old Lootsberg Pass is characteristic of the transitional mudrocks from the *Daptocephalus* to *Lystrosaurus* AZ and not reported previously. Both rock types exhibit primary structures of fluvial depositional processes, along with an array of bioturbation features associated with activity at both the sediment–water interface and in a vadose zone. Both rock types possess the same geochemical signature and differ only in color, which is a function of hematite coatings on clay minerals. And, similar to conclusions drawn from other studies on red-colored mudrock (e.g., Picard 1965; Dubiel and Smoot 1994; Kraus 1997; Sheldon 2005), we find no physical, geochemical, or rock-magnetic evidence to support the currently accepted model (Ward et al. 2005; Smith and Botha-Brink 2014; Rubidge et al. 2016; Viglietti et al. 2016) that their coloration is related to an increasingly arid climatic setting across the vertebrate assemblage-zone transition. Our data indicate that the landscape in the earliest part of the *Lystrosaurus* Assemblage Zone was wet, and allowed for the continued growth of a Permian-age flora under conditions of high water table that experienced temporal fluxes in the hydrological regime promoting spatial color modification of sediment.

SUPPLEMENTAL MATERIAL

Supplemental text and 4 tables are available from JSR's Data Archive: <http://sepm.org/pages.aspx?pageid=229>.

ACKNOWLEDGMENTS

The authors thank: D. Dyar and E. Sklute, Mount Holyoke College, for providing Mössbauer spectroscopic data; M. Yates, University of Maine-Orono, for assistance with SEM imaging and EDS spectroscopy; N. Tabor, L. Michel, and R. Beavers, Southern Methodist University, who provided help with clay mineralogy; and B. Rueger, Colby College, for assistance with clay-slide preparation. T. Sasajima and K. Lipshultz, Colby College, are acknowledged for field assistance. K. Ables and M. Abdulkadir, UT Dallas, are thanked for their

assistance with rock-magnetism measurements. We are grateful for comments from two anonymous reviewers. Support for fieldwork and laboratory analyses was provided by Department of Geology Endowment funds, Office of the Provost and Dean of Faculty, Presidential Scholars Opportunity Grant, start-up funds to JWG, and Whipple-Coddington Endowment and National Science Foundation funding to RAG (NSF EAR 1123570 and 1624302).

REFERENCES

- BALDOCK, J.A., 2002, Interactions of organic materials and microorganisms with minerals in the stabilization of soil structure, *in* Huang, P.M., Bollag, J.M., and Senesi, N., eds., *Interactions between Soil Particles and Microorganisms: Impact on the Terrestrial Ecosystem*: New York, Wiley and Sons, p. 134–188.
- BASU, A.R., PETAEV, M.I., POREDA, R.J., JACOBSEN, S.B., AND BECKER, L., 2003, Chondritic meteorite fragments associated with the Permian–Triassic boundary in Antarctica: *Science*, v. 302, p. 1388–1392.
- BEHRENSMEYER, A.K., KIDWELL, S.M., AND GASTALDO, R.A., 2000, Taphonomy and paleobiology: *Paleobiology*, v. 26, p. 103–147.
- BEITLER, B., CHAN, M.A., AND PARRY, W.T., 2003, Bleaching of Jurassic Navajo Sandstone on Colorado Plateau Laramide highs: evidence of exhumed hydrocarbon supergiants?: *Geology*, v. 12, p. 1041–1044.
- BENISON, K.C., BOWEN, B.B., OBOH-IKUENOBE, F.E., JAGNIECKI, E.A., LACLAIR, D.A., STORY, S.L., MORMILE, M.R., AND HONG, B.-Y., 2007, Sedimentology of acid saline lakes in southern western Australia: newly discovered processes and products of an extreme environment: *Journal of Sedimentary Research*, v. 77, p. 366–388.
- BENTON, M.J., AND NEWELL, A.J., 2014, Impact of global warming on Permo-Triassic terrestrial ecosystems: *Gondwana Research*, v. 25, p. 1308–1337.
- BOTHA, J., AND SMITH, R.H.M., 2006, Rapid vertebrate recuperation in the Karoo Basin of South Africa following the End-Permian extinction: *Journal of African Earth Sciences*, v. 45, p. 502–514.
- BOTHA, J., AND SMITH, R.H.M., 2007, *Lystrosaurus* species composition across the Permo-Triassic boundary in the Karoo Basin of South Africa: *Lethaia*, v. 40, p. 125–137.
- BURGESS, S.D., BOWRING, S., AND SHEN, S., 2014, High-precision timeline for Earth's most severe extinction: *National Academy of Science, Proceedings*, v. 111, p. 3316–3321.
- CONEY, L., REIMOLD, W.U., HANCOX, J., MADER, D., KOEBERL, C., McDONALD, I., STRUCK, U., VAJDA, V., AND KAMO, S.L., 2007, Geochemical and mineralogical investigation of the Permian–Triassic boundary in the continental realm of the southern Karoo Basin, South Africa: *Paleoworld*, v. 16, p. 67–104.
- DE KOCK, M.O., AND KIRSCHVINK, J.L., 2004, Paleomagnetic constraints on the Permian–Triassic boundary in terrestrial strata of the Karoo Supergroup, South Africa: implications for causes of the End-Permian Extinction Event: *Gondwana Research*, v. 7, p. 175–183.
- DI MICHELE, W.A., AND GASTALDO, R.A., 2008, Plant paleoecology in deep time: *Missouri Botanical Garden Annals*, v. 95, p. 144–198.
- DOORNENBAL, H., AND STEVENSON, A., 2010, *Petroleum geological atlas of the southern Permian basin area*: European Association of Geoscientists and Engineers Publications, Houston, 342 p.
- DROSER, M.L., AND BOTTJER, D.J., 1986, A semiquantitative field classification of ichnofabric: *Journal of Sedimentary Petrology*, v. 56, p. 558–559.
- DUBIEL, R., AND SMOOT, J.P., 1994, Criteria for interpreting paleoclimate from red beds: a tool for Pangean Reconstructions: *Canadian Society of Petroleum Geologists, Memoir 17*, p. 295–310.
- ERWIN, D.H., 2006, *Extinction: How Life on Earth Nearly Ended 250 Million Years Ago*: Princeton, N.J., Princeton University Press, 320 p.
- EVANS, M.E., AND HELLER, F., 2001, Magnetism of loess/paleosol sequences: recent developments: *Earth-Science Reviews*, v. 54, p. 129–144.
- GASTALDO, R.A., AND DEMKO, T.M., 2011, The relationship between continental landscape evolution and the plant-fossil record: long term hydrology controls the plant fossil record, *in* Allison, P.A., and Bottjer, D.J., eds., *Taphonomy, Second Edition: Processes and Bias Through Time*: Springer, The Netherlands, Topics in Geobiology, v. 32, p. 24–286.
- GASTALDO, R.A., AND NEVELING, J., 2012, The terrestrial Permian–Triassic boundary event is a nonevent: Reply: *Geology*, v. 40, p. e257, doi:10.1130/G32975Y.1.
- GASTALDO, R.A., AND NEVELING, J., 2016, Comment on “Anatomy of a mass extinction: sedimentological and taphonomic evidence for drought-induced die-offs at the Permo-Triassic boundary in the main Karoo Basin, South Africa” by R.M.H. Smith and J. Botha-Brink: *Palaeogeography, Palaeoclimatology, Palaeoecology*, v. 396, p. 99–118.
- GASTALDO, R.A., AND ROLERSON, M.W., 2008, *Katbergia* gen. Nov., a new trace fossil from Upper Permian and Lower Triassic rocks of the Karoo Basin: implications for palaeoenvironmental conditions at the P/Tr extinction event: *Palaeontology*, v. 51, p. 215–229.
- GASTALDO, R.A., BEARCE, S.C., DEGGES, C., HUNT, R.J., PEEBLES, M.W., AND VIOLETTE, D.L., 1989, Biostratigraphy of a Holocene oxbow lake: a backswamp to mid-channel transect: Review of Palaeobotany and Palynology, v. 58, p. 47–60.
- GASTALDO, R.A., NEVELING, J., CLARK, K., AND NEWBURY, S.S., 2009, The terrestrial Permian–Triassic boundary event bed is a non-event: *Geology*, v. 37, p. 199–202.

- GASTALDO, R.A., PLUDOW, B.A., AND NEVELING, J., 2013, Mud aggregates from the Katberg Formation, South Africa: additional evidence for Early Triassic degradational landscapes: *Journal of Sedimentary Research*, v. 83, p. 531–540.
- GASTALDO, R.A., KNIGHT, C.L., NEVELING, J., AND TABOR, N.J., 2014, Latest Permian paleosols from Wapadberg Pass, South Africa: implications for Changhsingian climate: *Geological Society of America, Bulletin*, v. 126, p. 665–679.
- GASTALDO, R.A., KAMO, S.L., NEVELING, J., GEISSMAN, J.W., BAMFORD, M., AND LOOY, C.V., 2015, Is the vertebrate-defined Permian–Triassic boundary in the Karoo Basin, South Africa, the terrestrial expression of the end-Permian marine event?: *Geology*, v. 43, p. 939–942.
- GASTALDO, R.A., NEVELING, J., LOOY, C.V., BAMFORD, M.K., KAMO, S.L., AND GEISSMAN, J.W., 2017, Paleontology of the Blaauwater 67 and 65 Farms, South Africa: testing the *Daptocephalus/Lystrosaurus* biozone boundary in a stratigraphic framework: *Palaios*, v. 34, p. 369–366.
- GEOLOGICAL SOCIETY OF AMERICA, 2008, The Geological Society of America Rock-Color Chart with genuine Munsell color chips: Boulder, Colorado, Geological Society of America, 10 p.
- JOHNSON, M.R., VAN VUUREN, C.J., VISSER, J.N.J., COLE, D.I., WICKENS, H.DEV., CHRISTIE, A.D.M., ROBERTS, D.L., AND BRANDL, G., 2006, Sedimentary rocks of the Karoo Supergroup, in Johnson, M.R., Anhaeusser, C.R., and Thomas, R.J., eds., *The Geology of South Africa: The Geological Society of South Africa, Johannesburg, and The Council for Geoscience, Pretoria*, p. 461–499.
- JOHNSTON, J.H., AND CARDILE, C.M., 1987, Iron substitution in montmorillonite, illite, and glauconite by ^{57}Fe Mössbauer Spectroscopy: *Clays and Clay Minerals*, v. 35, p. 170–176.
- KELLER, W.D., 1953, Illite and montmorillonite in green sedimentary rocks: *Journal of Sedimentary Petrology*, v. 23, p. 3–9.
- KÖHLER, S.J., DUFAUD, F., AND OELKERS, E.H., 2003, An experimental study of illite dissolution kinetics as a function of pH from 1.4 to 12.4 and temperature from 5 to 50°C: *Geochimica et Cosmochimica Acta*, v. 67, p. 3583–3594.
- KRAUS, M., 1997, Lower Eocene alluvial paleosols: pedogenic development, stratigraphic relationships, and paleosol/landscape associations: *Palaeogeography, Palaeoclimatology, Palaeoecology*, v. 129, p. 387–406.
- KRAUS, M.J., AND HASIOTIS, S.T., 2006, Significance of different modes of rhizolith preservation to interpreting paleoenvironmental and paleohydrologic settings: examples from Paleogene paleosols, Bighorn Basin, Wyoming, USA: *Journal of Sedimentary Research*, v. 76, p. 633–646.
- MACLEOD, K.G., SMITH, R.M.H., KOCH, P.L., AND WARD, P.D., 2000, Timing of mammal-like reptile extinctions across the Permian–Triassic boundary in South Africa: *Geology*, v. 28, p. 227–230.
- MÜCHER, H.J., AND DE PLOEY, J., 1990, Sedimentary Structures formed in eolian-deposited silt loams under simulated conditions on dry, moist and wet surfaces: Amsterdam, Elsevier, *Developments in Soil Science*, v. 19, p. 155–160.
- MUNSELL SOIL COLOR CHART, 2000, GrelgMacbeth, New Windsor, New York, 28 p.
- MURAD, E., AND WAGNER, U., 1994, The Mössbauer spectrum of illite: *Clay Minerals*, v. 29, p. 1–10.
- NESSE, W.D., 2012, *Introduction to Mineralogy*: New York, Oxford University Press, 480 p.
- NEVELING, J., GASTALDO, R.A., KAMO, S.L., GEISSMAN, J.W., LOOY, C.V., AND BAMFORD, M.K., 2016, A review of stratigraphic, geochemical, and paleontological correlation data of the terrestrial end-Permian record in the Karoo Basin, South Africa, in de Wit, M., and Linol, B., eds., *The Origin and Evolution of the Cape Mountains and Karoo Basin*: Berlin, Springer Publishing, p. 151–157.
- OTTONE, G., MONTI, M., MARSICANO, C., AND MANCUSO, A.C., 2014, A new Late Triassic age for the Puesto Viejo Group (San Rafael depocenter, Argentina): SHRIMP U–Pb zircon dating and biostratigraphic correlations across southern Gondwana: *Journal of South American Earth Sciences*, v. 56, p. 186–199.
- PACE, D.W., GASTALDO, R.A., AND NEVELING, J., 2009, Early Triassic aggradational and degradational landscapes of the Karoo Basin and evidence for climate oscillation following the P-Tr event: *Journal of Sedimentary Research*, v. 79, p. 316–331.
- PARRISH, J.T., 1998, *Interpreting Pre-Quaternary Climate from the Geologic Record*: New York, Columbia University Press, 338 p.
- PAYNE, J.L., AND CLAPHAM, M.E., 2012, End-Permian Mass Extinction in the oceans: an ancient analog for the twenty-first century?: *Annual Review of Earth and Planetary Sciences*, v. 40, p. 89–111.
- PICARD, M.D., 1965, Iron oxides and fine-grained rocks of Red Peak and Crow Mountain sandstone members, Chugwater (Triassic) Formation, Wyoming: *Journal of Sedimentary Petrology*, v. 35, p. 464–479.
- PREVEC, R., GASTALDO, R.A., NEVELING, J., REID, S.B., AND LOOY, C.V., 2010, An autochthonous glossopterid flora with latest Permian palynomorphs from the *Dicynodon* Assemblage Zone of the southern Karoo Basin, South Africa: *Palaeogeography Palaeoclimatology Palaeoecology*, v. 292, p. 381–408.
- RETALLACK, G.J., 2001, *Soils of the Past: An Introduction to Paleopedology*, Second Edition: New York, Wiley, 404 p.
- RETALLACK, G.J., 2005, Earliest Triassic claystone breccias and soil-erosion crisis: *Journal of Sedimentary Research*, v. 75, p. 679–695.
- RETALLACK, G.J., SMITH, R.M.H., AND WARD, P.D., 2003, Vertebrate extinction across Permian–Triassic boundary in Karoo Basin, South Africa: *Geological Society of America, Bulletin*, v. 115, p. 1133–1152.
- REY, K., AMIOT, R., FOUREL, F., RIGAUDIER, T., ABDALA, F., DAY, M.O., FERNANDEZ, V., FLUTEAU, F., FRANCE-LANORD, C., RUBIDGE, B.S., SMITH, R.M., VIGLIETTI, P.A., ZIPPEL, B., AND LÉCUYER, C., 2016, Global climate perturbations during the Permo-Triassic mass extinctions recorded by continental tetrapods from South Africa: *Gondwana Research*, v. 37, p. 384–396.
- ROBB, G.L., 1949, Red bed coloration: *Journal of Sedimentary Petrology*, v. 19, p. 99–103.
- RUBIDGE, B.A., HANCOX, P.J., AND CATUNEANU, O., 2000, Sequence analysis of the Ecca–Beaufort contact in the southern Karoo of South Africa: *South African Journal of Geology*, v. 103, p. 81–96.
- RUBIDGE, B.S., DAY, M.O., BARBOLINI, N., HANCOX, P.J., CHOINIERE, J., BAMFORD, M.K., VIGLIETTI, P.A., MCPHEE, B., AND JIRAH, S., 2016, Advances in nonmarine Karoo biostratigraphy: significance for understanding basin development, in de Wit, M., and Linol, B., eds., *The Origin and Evolution of the Cape Mountains and Karoo Basin*: Berlin, Springer Publishing, Chapter 19, p. 141–150.
- SCHWERTMANN, U., FRIEDL, J., AND STANJEK, H., 1999, From Fe(III) ions to ferrihydrite and then to hematite: *Journal of Colloidal and Interface Science*, v. 209, p. 215–223.
- SHELDON, N.D., 2005, Do red beds indicate paleoclimatic conditions?: a Permian case study: *Palaeogeography, Palaeoclimatology, Palaeoecology*, v. 228, p. 305–319.
- SHELDON, N.D., AND TABOR, N.J., 2009, Quantitative paleoenvironmental and paleoclimatic reconstruction using paleosols: *Earth-Science Reviews*, v. 95, p. 1–52.
- SMITH, R.M.H., 1980, The lithology, sedimentology and taphonomy of flood-plain deposits of the Lower Beaufort (Adelaide Subgroup) strata near Beaufort West: *Geological Society of South Africa, Transactions*, v. 83, p. 399–413.
- SMITH, R.M.H., 1990, Alluvial paleosols and pedofacies sequences in the Permian Lower Beaufort of the southwestern Karoo Basin, South Africa: *Journal of Sedimentary Petrology*, v. 60, p. 258–276.
- SMITH, R.M.H., 1993, Sedimentology and ichnology of floodplain paleofacies in the Beaufort Group (Late Permian), Karoo Sequence, South Africa: *Palaios*, v. 8, p. 339–357.
- SMITH, R.M.H., 1995, Changing fluvial environments across the Permian–Triassic boundary in the Karoo Basin, South Africa and possible causes of tetrapod extinctions: *Palaeogeography, Palaeoclimatology, Palaeoecology*, v. 117, p. 81–104.
- SMITH, R.M.H., AND BOTHA, J., 2005, The recovery of terrestrial vertebrate diversity in the South African Karoo Basin after the end-Permian Extinction: *Compte Rendu Palevol*, v. 4, p. 555–568.
- SMITH, R.M.H., AND BOTHA-BRINK, J., 2014, Anatomy of a mass extinction: sedimentological and taphonomic evidence for drought-induced die-offs at the Permo-Triassic boundary in the main Karoo Basin, South Africa: *Palaeogeography, Palaeoclimatology, Palaeoecology*, v. 396, p. 99–118.
- SMITH, R.M.H., AND WARD, P.D., 2001, Pattern of vertebrate extinctions across an event bed at the Permian–Triassic boundary in the Karoo Basin of South Africa: *Geology*, v. 29, p. 1147–1150.
- TABOR, N.J., AND MONTAÑEZ, I.P., 2004, Morphology and distribution of soils in the Permo-Pennsylvanian Wichita and Bowie Groups, north-central Texas, USA: implications for western equatorial Pangean paleoclimate during icehouse–greenhouse transition: *Sedimentology*, v. 51, p. 851–884.
- THOMPSON, A.M., 1970, Geochemistry of color genesis in red-bed sequence, Juniata and Bald Eagle formations, Pennsylvania: *Journal of Sedimentary Petrology*, v. 40, p. 599–615.
- TURNER, P., 1980, *Continental Red Beds: Developments in Sedimentology* 29, Elsevier, 562 p.
- VELDE, B., AND MEUNIER, A., 2008, *The Origin of Clay Minerals in Soils and Weathered Rocks*: Berlin, Springer-Verlag, 606 p.
- VIGLIETTI, P.A., SMITH, R.M.H., ANGIELCZYK, K.D., KAMMERER, C.F., FRÖBISCH, J., AND RUBIDGE, B.S., 2016, The *Daptocephalus* Assemblage Zone (Lopingian), South Africa: a proposed biostratigraphy based on a new compilation of stratigraphic ranges: *Journal of African Earth Sciences*, v. 113, p. 153–164.
- WARD, P.D., MONTGOMERY, D.R., AND SMITH, R.M.H., 2000, Altered river morphology in South Africa related to the Permian–Triassic extinction: *Science*, v. 289, p. 1740–1743.
- WARD, P.D., BOTHA, J., BUICK, R., DE KOCK, M.O., ERWIN, D.H., GARRISON, G.H., KIRSCHVINK, J.L., AND SMITH, R.M.H., 2005, Abrupt and gradual extinction among Late Permian land vertebrates in the Karoo Basin, South Africa: *Science*, v. 307, p. 709–714.

Received 3 January 2017; accepted 27 April 2017.